Eidgenössische Technische Hochschule Zürich
Swiss Federal Institute of Technology Zurich

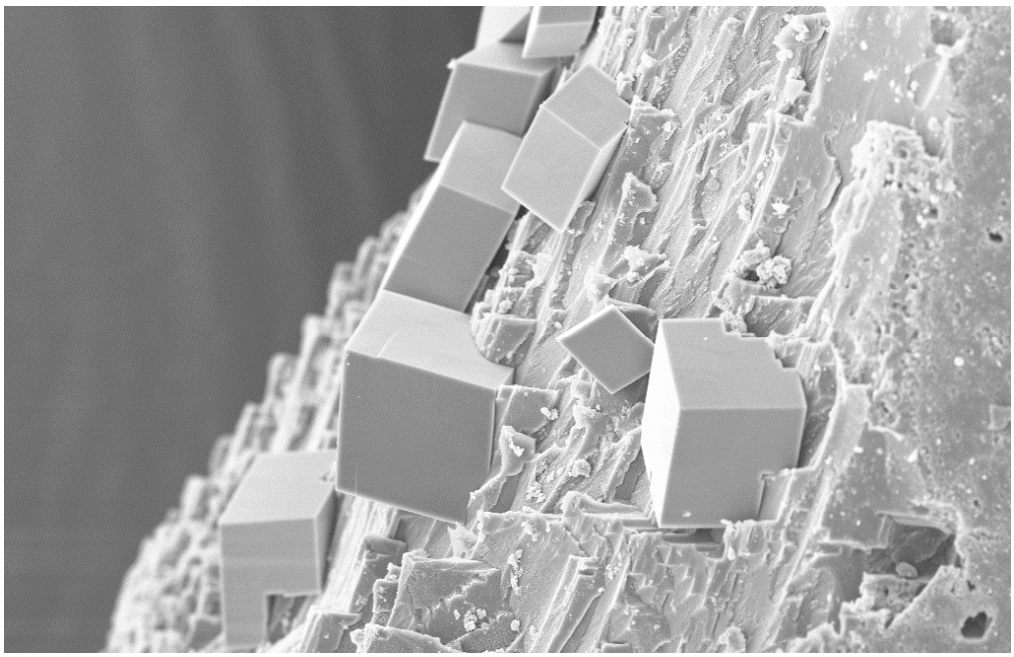

Aqueous Mineral Carbonation

Precipitating Magnesite from Olivine

Diploma Thesis

submitted to:
Prof. Dr. Marco Mazzotti
Separation Processes Laboratory
Institute of Process Engineering
D-MAVT, ETH ZURICH

for receiving the Diploma in Environmental Sciences

by:
Mischa Werner

Zurich – August 25th, 2008

Distribution:

Dr. Marco Mazzotti, ETH Zurich

Dr. Nicolas Gruber, ETH Zurich

Dr. Valentina Prigiobbe, ETH Zurich

August 25th 2008, print version

Author:	Mischa Werner Limmattalstrasse 52 CH-8049 Zurich miswerne@ethz.ch
Supervisior D-MAVT	Prof Dr Marco Mazzotti Institute of Process Engineering Separation Processes Laboratory ETH-Zurich, Switzerland marco.mazzotti@ipe.mavt.ethz.ch
Co-Supervisior D-UWIS	Prof Dr Nicolas Gruber Institute of Biogeochemistry & Pollutant Dynamics Professorship for Environmental Physics ETH Zurich, Switzerland nicolas.gruber@env.ethz.ch
Co-Supervisior D-MAVT	Dr Valentina Prigiobbe Institute of Process Engineering Separation Processes Laboratory ETH-Zurich, Switzerland valentina.prigiobbe@ipe.mavt.ethz.ch

Front page illustration: Crystals on olivine surface, precipitated during experiment R143 on May 23rd, 2008

Abstract

Mineral carbonation is a young field of research with the potential to fix anthropogenic CO_2 safely and permanently in solid carbonates. The aqueous mineral carbonation process has been investigated on the basis of a modeling approach and experimental work. A population balance equation model has been developed and its solution was coupled with a reactor model. Olivine dissolution was modeled with a pH-depending rate law. Kinetic expressions with conceptual parameters for heterogeneous nucleation and isotropic growth were applied for the precipitation of magnesite. Speciation for the H_2O-CO_2-olivine system was modeled using a reduced set of reactions under the assumption of immediate equilibration for dissociation and complexation reactions. A sensitivity analysis identified the overall model to be most sensitive to the reactor temperature.

Experiments were carried out in a flow-through reactor at 120°C and under a CO_2 atmosphere of 100 bar, using a particle size fraction of San Carlos olivine between 90 and 180 μm. Supersaturation and the formation of complexes have been calculated using the geochemical software package EQ3/6. The model failed to describe the measured concentration profile for magnesium in experiments with a solid-liquid ratio of 5%. The validity of the employed dissolution rate was confirmed at low concentration levels. Dissolution was measured to be stoichiometric with respect to silicon and magnesium also at higher concentrations. Hence the fine-grained secondary phase observed on distinct parts of the reacted particles did not contain magnesite and silica. Instead, very low Fe:Mg ratios in the reactor solution indicated the precipitation of iron-oxides. This could have hindered the olivine dissolution and thus account for the overestimation of the true magnesium concentration by the model. Problems with the experimental set-up prevented a further testing of this hypothesis. Future work should investigate the role of iron-oxide precipitation on the dissolution of olivine and thus on the performance of the overall mineral carbonation process.

Acknowledgments

First and foremost, I would like to thank Prof Marco Mazzotti for his guidance and support throughout the work progress; for the time he invests in us master students, which is something I don't take for granted. I also like to take the occasion to sincerely thank him for his trust, and for helping me closing the gap between the science- and engineering-background. I learned a whole lot during the last six months, which is priceless!

I would also like to thank Prof Nicolas Gruber for being my co-supervisor at the D-UWIS and thus eliminating the administrative barriers that arise when doing a diploma thesis at another department.

Major thanks go to my co-supervisor and future co-worker here at the Separation Process Laboratory, Dr. Valentina Prigiobbe, for the discussions, the initial support to get familiar with the lab and experimental work and the valuable tips regarding this thesis.

A nonstandard financial support from the Scholarship Office of the ETH Zurich is gratefully acknowledged. During this intensive time it was impossible to continue my part-time job; the help I received from the ETH was fast and uncomplicated.

A special thank goes to my dear friends and work mates Mike Grendelmeier and Christoph Marugg, who were the first to grasp my situation and initiated the successful funding.

Table of contents page

List of figures page

List of tables page

1. Introduction

Motivation

Fighting the rise in atmospheric carbon dioxide (CO_2) concentration has become the world's crucial task in order to prevent global warming higher than 2°C relative to pre-industrial times. A temperature increase in this order of magnitude is believed to border major changes in ecosystems with predominantly negative consequences (IPCC WGII, 2007). In fact, the economical and ecological loss is hardly predictable. The quest for counter strategies is urgent, since global average surface temperature has already increased by 0.74 °C during the last 100 years (IPCC WGI, 2007).

Carbon dioxide Capture and Storage

Realistically, this task needs a broad portfolio of mitigation options. A novel approach is Carbon Dioxide Capture and Storage (CCS), which is defined as the collection of CO_2 from large point sources (or ambient air) and its storage in suitable reservoirs, including the logistical challenge of transport, site selection and site management (IPCC SRCCS, 2005). CCS is the only way to bring carbon from the living pool, including the biosphere, hydrosphere, and atmosphere, back into the dead pool, i.e. the lithosphere, where it has been extracted by humans at a speed the climate system cannot cope with anymore. In terms of pollution control, capturing emissions and storing them suitably signifies traditional end-of-pipe thinking, labeled the wrong approach by critics. However, since the International Panel on Climate Change (IPCC) published a special report on CCS in 2005, this technology is widely regarded as a potentially important mitigation option:

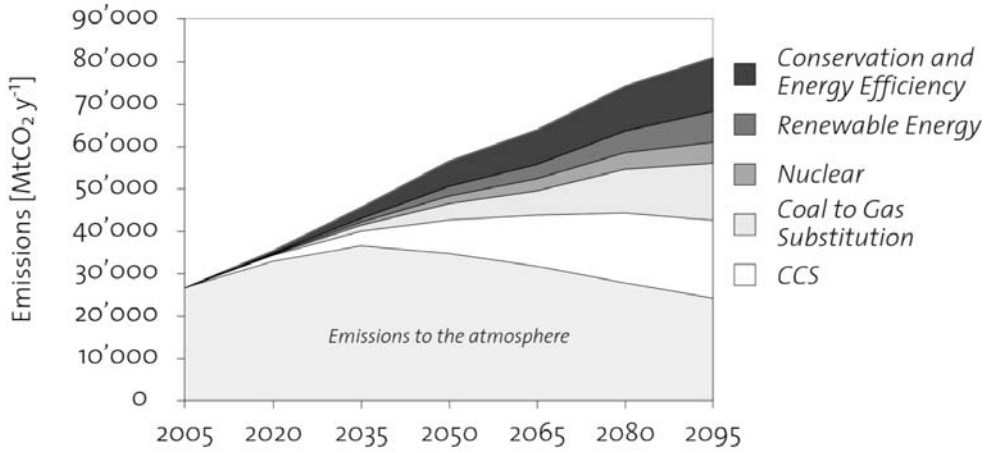

Figure 1-1: The global CO_2 emissions and corresponding contributions of main emission reduction measures in the current mitigation portfolio (IPCC SRCC, 2005).

1.1. Mineral Carbonation

Geological storage

Several technological options exist within the concept of CCS. Comparing global storage capacities and current CO_2 emissions reveals only two options with the potential for a save disposal over centuries. This is on the one hand geological storage, where a thick enough cap rock with adequate sealing qualities together with in-situ physical and chemical trapping mechanisms are believed to guarantee a save and permanent retention (IPCC SRCCS, 2005).

Definition and potential

On the other hand, mineral carbonation refers to the geological fixation of CO_2 ex-situ in a chemical processing plant, using alkaline and alkaline-earth oxides, such as magnesium oxide (MgO) and calcium oxide (CaO), to convert gaseous CO_2 into solid carbonates such as magnesium carbonate ($MgCO_3$) and calcium carbonate ($CaCO_3$) (IPCC SRCCS, 2005, Chapter 7). The carbonation reaction takes place in a reactor under controllable conditions that are optimized to meet maximal conversion efficiency at minimal costs. The feed oxides are present in silicate minerals such as olivine ($(Mg,Fe)_2SiO_4$), serpentine ($(Mg,Fe,Ni)_3Si_2O_5(OH)_4$) or wollastonite ($CaSiO_3$). Naturally occurring reservoirs of these minerals provide the quantity of oxides needed to fix all CO_2 that would be emitted by the combustion of the worldwide available fossil fuel reserves (IPCC SRCCS, 2005). The same oxides can be found in industrial residues, namely in steel slag, fly ash and waste concrete. These materials are more reactive than the natural minerals, but available only in small quantities (IPCC SRCCS, 2005).

Fundamentals of the process

Mineral carbonation can be performed either by solid-gas reaction or in an aqueous system, the latter being more efficient (e.g. Zevenhoven et al., 2006). In the case of water being the solvent, the CO_2 lowers the pH by forming carbonic acid (H_2CO_3), which dissociates to bicarbonate (HCO_3^-) and carbonate (CO_3^{2-}) after the following reaction:

$$CO_2 + H_2O \longleftrightarrow H_2CO_3 \longleftrightarrow H^+ + HCO_3^- \longleftrightarrow 2H^+ + CO_3^{2-} \quad (1)$$

The liberated protons cause the dissolution of the feed material, as exemplified by the dissolution reaction of forsterite (Mg_2SiO_4):

$$Mg_2SiO_4 + 4H^+ \longleftrightarrow 2Mg^{2+} + SiOH_4^\circ \quad (2)$$

The detached ionic species can then react with the deprotonated carbonic acid to form solid carbonate minerals:

$$Mg^{2+} + CO_3^{2-} \longleftrightarrow MgCO_3 \quad (3)$$

The reaction products, i.e. unreacted feed material, carbonates, and silica (SiO_2), have to be stored suitably, for example in depleted mines. In an ideal mineral carbonation scheme, the reactor is located next to the power plant with a nearby silicate quarry, in order to avoid transportation. Moreover, the water use and treatment of the

reactor solution are key features in order to keep the process environmentally benign. This is of special importance if additives such as sodium bicarbonate ($NaHCO_3$) and sodium chloride (NaCl) are used to increase the activity of the species involved.

Background

The overall reaction (reactions 1-3) is with 72.9 kJ mol^{-1} slightly exothermic and thus a spontaneously occurring natural process. On a geological time scale, it plays a key role in silicate weathering and the formation of secondary minerals. Solidifying magma causes a steady CO_2 flux into overlying formations, where it comes to silicate weathering and carbonate precipitation, as part of the global carbon cycle. (e.g. Lasaga, 1981; Berner and Lasaga, 1989). This process is slow, but ever lasting. Using it to sequester CO_2 was first proposed by Seifritz (1990) and initially investigated by Dunsmore (1992), Gunter et al. (1993), Bachu et al. (1994) and Lackner et al. (1995), to name a few amongst others.

Challenge and mineral pretreatment

To accelerate the overall mineral carbonation process is the primary objective of today's research. Besides using additives as aforementioned, the speed of reaction can be improved by increasing the CO_2 pressure and reactor temperature, whereas the latter may not exceed 185°C, since the exothermic overall reaction was found to become thermodynamically unfavorable above this temperature (McKelvy et al. 2006). Improving the reactivity of the feed material is achieved either by thermal or mechanical pretreatment (grinding and milling). While the former removes chemically bound water, the latter reduces the mean particle size. Both methods primarily lead to an increased surface area and thus to a faster dissolution of the feed material. However, such activation can only be achieved under a substantial energy penalty that is most critical to the viability of any mineral-carbonation process (O'Conner et al., 2005).

2. Modeling

2.1. Population balance equation model

Population balance equation

In terms of particulate processes theory, aqueous mineral carbonation is divided into three main crystallization phenomena:

1. particle dissolution
2. nucleation
3. crystal growth

In order to describe these three processes in a compact representation and to gain the theoretical understanding about their interconnection, a population balance equation (PBE) model was developed. A PBE describes the number of crystals in a given size range ΔL over the time interval Δt. Crystal size is parameterized using a characteristic particle length L, which has to be related to a physical property of the particles. It is convenient to use Feret diameters, i.e. the distance of two parallel tangent planes on a particle.

Particle size distribution

The number of crystals can then be expressed by the particle size distribution (PSD):

$$n(t,L) = \frac{dN}{dL}. \tag{4}$$

The PSD represents the unscaled number distribution density of the particle population. With $N(L)$ being the cumulative particle size distribution, $n(t,L)dL$ returns the concentration of particles at given time t in the size range L to $L + dL$.

Particle shape

For the sake of simplicity, spatial complexity of the true particle shape was reduced to a 1-D model, characterizing size and shape simultaneously using only one parameter, i.e. L. Therefore, dimensionless shape factors, k_a and k_v, were defined to relate the square and the cube of side length L to its surface a and volume v (Randolph and Larsson, 1988):

$$a = k_a L^2, \tag{5}$$

$$v = k_v L^3. \tag{6}$$

Generally, k_a and k_v have to be estimated from image analysis for each kind of particles. In the context of a 1-D model, they are assumed to be time-invariant and size-independent, which is only true under the constraint of isotropic dissolution and growth.

Moments of a distribution

The total surface area $A(t)$ and volume $V(t)$ for a given particle population can be derived by introducing the concept of the moments of a distribution. The jth moment of the PSD of the ith material, $n_i(t,L_i)$, is defined as:

$$\mu_i^j(t) = \int_0^\infty L^j n_i(t,L_i)dL. \tag{7}$$

Only the first four moments are related to a physical meaning, namely the zeroth (μ_i^0) to the total number of particles, the first (μ_i^1) to the cumulative length of all particles, the second (μ_i^2) to the total surface area and the third (μ_i^3) to the total volume of the population. Using these properties, one can write:

$$A_i(t) = k_{a,i}\mu_i^2(t), \tag{8}$$

$$V_i(t) = k_{v,i}\mu_i^3(t). \tag{9}$$

Dissolution, growth, nucleation, birth and death events

The definition of the dissolution rate *R* and growth rate *G* is given by the infinitesimal change of L over time (m s^{-1}), which is negative for *R* and positive for *G*, respectively:

$$R = G = \frac{dL}{dt}. \tag{10}$$

Recalling the definition of *N(L)* from Eq. (4), the nucleation rate *J* is defined as the change of the number of particles over time at *L* = 0:

$$J = \left.\frac{dN}{dt}\right|_{L=0}. \tag{11}$$

At *L* > 0, the net appearance of particles is given by (*B*(*L*) - *D*(*L*))*dL*, with *B*(*L*) representing birth events such as agglomeration or aggregation and *D*(*L*) being death events such as breakage. To focus on the fundamentals of the mineral carbonation process, the occurrence of birth and death events was neglected.

Final population balances

Thus, the final population balances write (Randolph and Larson, 1988):

$$\frac{\partial n_d}{\partial t} - R\frac{\partial n_d}{\partial L_d} = 0, \tag{12}$$

$$\frac{\partial n_p}{\partial t} - G\frac{\partial n_p}{\partial L_p} = 0, \tag{13}$$

with subscript *d* and *p* indicating the dissolution and precipitation part, respectively. Initial and boundary conditions for the two homogeneous partial differential equations (first-order wave equations) are:

$$n_d(0,L_d) = n_d^0(L_d), \tag{14}$$

$$n_d(t,0) = 0, \tag{15}$$

$$n_p(0,L_p) = 0, \tag{16}$$

$$n_p(t,0) = \frac{J}{G}, \tag{17}$$

Reactor model

The solution to the PBEs was coupled with a reactor model. A mass balance for the concentration of the total magnesium in solution, $c_{Mg(aq)}$ (mol l^{-1}, M), was formulated to be applicable either for a batch reactor or a continuous flow stirred tank reactor (CFSTR). It is given by:

$$V\frac{dc_{Mg(aq)}}{dt} = \nu\frac{dm_d}{dt} - \frac{dm_p}{dt} - Qc_{Mg(aq)}, \tag{18}$$

where V (ml) is the liquid volume in the reactor, ν is the number of moles of magnesium in one mole of olivine, m_d and m_p (mol) are the masses of solute and precipitate, and Q (ml min^{-1}) is the flow rate through the reactor. In the case of Q equal to 0, Eq. (18) refers to a mass balance for a batch system, otherwise to a CFSTR system.

Method of moments

The partial differential equations (12) and (13) have been solved using the method of moments. The two PBEs were transformed into a set of coupled ordinary differential equations (ODEs), consisting of the time derivatives of the first four moments of the PSD. Starting with the zeroth moment, this writes for the olivine dissolution:

$$\frac{d\mu_d^0}{dt} = Rn_d^0(\lambda), \tag{19}$$

$$\frac{d\mu_d^1}{dt} = R\mu_d^0, \tag{20}$$

$$\frac{d\mu_d^2}{dt} = 2R\mu_d^1, \tag{21}$$

$$\frac{d\mu_d^3}{dt} = 3R\mu_d^2, \tag{22}$$

with $n_d^0(\lambda)$ representing the number of particles at time t that are dissolving completely. The corresponding characteristic length λ follows from the integral of the dissolution rate R:

$$\lambda = \left|\int_0^t R dt\right|. \tag{23}$$

For the magnesite precipitation, the set of ODEs is given by:

$$\frac{d\mu_p^0}{dt} = J, \tag{24}$$

$$\frac{d\mu_p^1}{dt} = G\mu_p^0, \tag{25}$$

$$\frac{d\mu_p^2}{dt} = 2G\mu_p^1, \tag{26}$$

$$\frac{d\mu_p^3}{dt} = 3G\mu_p^2. \tag{27}$$

Final mass balance for reactor model

Using the time derivatives of the third moment in integral form, i.e. the total volume of the particles, the mass balance in Eq. (18) can be recasted as follows:

$$\frac{dc_{Mg(aq)}}{dt} = \nu 3k_{v,d}\rho_d R\int_0^\infty n_d L_d^2 dL - 3k_{v,p}\rho_p G\int_0^\infty n_p L_p^2 dL - \frac{Q}{V}c_{Mg(aq)}, \tag{28}$$

where ρ_d and ρ_p (mol m^{-3}) are the molar densities of olivine and magnesite, respectively. The ODEs in Eqs. (19) to (28) were solved using the Matlab ode15s solver.

2.2. Olivine dissolution

Dissolution mechanism

Numerous studies suggest olivine dissolution being stoichiometric, provided the solution is highly undersaturated with respect to olivine (Wogelius and Walther, 1991; Chen and Brantley, 2000; Rosso and Rimstidt, 2000; Oelkers, 2001). Accordingly, the dissolution rate is assumed to be independent of the bulk liquid phase concentration and not hindered by diffusion. A surface controlled dissolution mechanism also implies the independency from particle shape and size. The currently most accepted model for the dissolution of olivine under acidic conditions (Pokrovsky and Schott, 2000) suggests the detachment of magnesium from the crystal surface to take place via a proton exchange of Mg^{2+} ions, followed by the polymerization of partially protonated SiO_4 tetrahedra. Rate controlling is the subsequent penetration of protons into the Mg-depleted surface layer and its adsorption on silica dimers. Hence, the dissolution rate solely depends on the proton activity a_H, i.e. *R = f(pH)*.

General dissolution rate law

Hänchen et al. (2006) performed olivine dissolution experiments in a CFSTR setup at 90-150°C under nitrogen atmospheres from 15 to 180 bar. Using a simple shrinking particle model, the following general rate law was regressed for pH values between 2 and 8.5:

$$r = U a_{H^+}^{\alpha} \exp\left(\frac{-E_a}{RT}\right), \tag{29}$$

where the activation energy E_a was determined at 52.9 kJ mol^{-1}, the pre-exponential factor U = 0.0854 (+0.67 to -0.076) and the rate of reaction α = 0.46 ± 0.03.

Batch specific dissolution rate law

In a later study by the same authors (Hänchen et al. 2007), different size fractions of olivine were dissolved and a PBE model was used to refine the rate law in Eq. (29) under operating conditions of 120°C and 100bar of CO_2 pressure. Within the pH range from 2 to 6.5, the following correlation was regressed:

$$\log\left(\frac{\gamma r}{\gamma_{ref}}\right) = -\alpha pH - \hat{U}. \tag{30}$$

While the rate of reaction α remained unchanged, the parameter $\hat{U}$ was updated to 8.05 ± 0.13. The factor γ was introduced to compare batches with different olivine size fractions. It describes the characterization of the initial PSD for each size fraction and is given by (all parameters referring to olivine):

$$\gamma = \frac{a_{BET} M\, m_0}{3\rho\, k_v^{2/3} \mu^{2,0}}, \tag{31}$$

with a_{BET} (cm^2 g^{-1}) being the specific surface area of the olivine feed, determined using the BET method as it is commonly done (e.g. Pokrovsky and Schott, 2000), M (g mol^{-1}) the molar mass, m_0 (mol) the initial amount of olivine and ($\mu^{2,0}$) the total surface of

the particles prior to dissolution (t = 0). Dividing the product γr by the γ_{ref} of a reference batch makes the rate law given in Eq. (30) comparable to other studies about olivine dissolution.

Combined dissolution rate law

In this work, Eqs. (29) and (30) were combined in order to simulate different reactor temperatures. This yields:

$$\log\left(\frac{\gamma r}{\gamma_{ref}}\right) = -\alpha pH - \frac{E_a}{2.303RT} - \tilde{U}, \tag{32}$$

where the new parameter $\tilde{U}$ = 1.021 ± 0.13.

Transformation of r into R

Hänchen et al. (2007) also give the derivation of the transformation of r (mol m^{-2} s^{-1}) into the rate definition R (m s^{-1}) as used in PBE modeling. Applying again factor γ from Eq. (31), the correlation writes:

$$\left(k_{v,d}\right)^{1/3} R = \gamma r. \tag{33}$$

2.3. Magnesite precipitation: Kinetics of nucleation and growth

Definition of supersaturtion

Precipitation kinetics is mostly controlled by the supersaturation ratio, here defined as:

$$S = \left(\frac{Q_{ap}}{K_{sp}}\right)^{1/n_{aq}}, \tag{34}$$

where Q_{ap} represents the actual activity product, K_{sp} the solubility product and n_{aq}, is the number of aqueous species that are involved in the precipitation process (Söhnel and Garside, 1992). To scale S by the power of $1/n_{aq}$ is useful when comparing supersaturation ratios of ionic crystals that consist partly of the same aqueous species, but having a different stoichiometry regarding this species.

General kinetic expressions for nucleation and growth

In accordance with the principles of classical nucleation and crystal growth theory (Schöll et al., 2006; therein after Mersmann, 2001), the following general rate expressions for heterogeneous nucleation, J, and isotropic growth, G, have been applied:

$$J = k_j S_p^{7/3} \exp\left(\frac{-K_j}{\ln^2 S_p}\right), \tag{35}$$

$$G = k_g \left(1 - S_p\right)^{5/6} \exp\left(\frac{-K_g}{S_p - 1}\right). \tag{36}$$

Alternatively to the heterogeneous nucleation (or in combination) and readily applicable if using the method of moments, one can formulate a similar expression for nucleation on the surface of the olivine particles:

$$J_s = k_s \mu_d^2 \exp\left(\frac{-K_s}{\ln\left(S_p\right)}\right). \tag{37}$$

The pre-exponential factors $k_{j/g/s}$ and exponential factors $K_{j/g/s}$ can be obtained by parameter estimation (Schöll et al., 2006).

Precipitation study for magnesite

Hänchen et al. (2008) studied the effect of temperature and CO_2 pressure on the precipitation of magnesite and other minerals in the H_2O-CO_2-Na_2CO_3-$MgCl_2$ system, where sodium bicarbonate (Na_2CO_3) and magnesium chloride ($MgCl_2$) were used to prepare supersaturated solutions. At operating conditions of 120°C and 100 bar of CO_2 pressure, the authors found magnesite starting to precipitate between $S_{mag.}$ = 11.5 and $S_{mag.}$ = 21. The induction time, i.e. the time elapsed between supersaturation is established and the first nuclei are formed, was within a few minutes and became only a few seconds (spontaneous precipitation) for solutions with ratios up to $S_{mag.}$ = 33.

Conceptual parameters for magnesite nucleation and growth

These findings were taken as an orientation for choosing a starting point for the kinetic parameters in *J*. Appendix 1 contains visualizations showing how the parameters have been sought that allow for a fast nucleation between $S_{mag.}$ = 10 and 20. It is important to mention the limits of this approach, as the referred results were obtained in a system containing also sodium (Na^+) and chloride (Cl^-), two ions that will affect the precipitation kinetics by influencing the ionic strength and thus the activities of all species involved.
Parameters for the growth rate G were adopted from Schöll et al. (2006), being aware that in their study another solid, L-glutamic acid, was investigated. Again, this has to be understood as a starting point to run preliminary simulations.

Summary of kinetic parameters

The whole set of kinetic parameters chosen for the modeling of the overall mineral carbonation process in is summed up in Table 2-1:

Table 2-1: Summary of the set of kinetic parameters for the mineral carbonation reactor model.

parameter	preliminary value	unit	description
α	0.46 x 10^0	[–]	rate of reaction, dissolution
$\tilde{U}$	1.021 x 10^0	[–]	pre-exponential factor, dissolution
E_a	52.9 x 10^3	[J mol^{-1} K^{-1}]	activation energy, dissolution
k_j	1 x 10^{12}	[# m^{-3} s^{-1}]	pre-exponential factor, heterogeneous nucleation
K_j	2 x 10^2	[–]	exponential factor, heterogeneous nucleation
k_g	2.5 x 10^{-7}	[m s^{-1}]	pre-exponential factor, isotropic growth
K_g	9 x 10^{-2}	[–]	exponential factor, isotropic growth
k_s	1 x 10^{22}	[# m^{-3} s^{-1}]	pre-exponential factor, surface nucleation
K_s	1.25 x 10^2	[–]	exponential factor, surface nucleation

Silica and other precipitates

Magnesite is not the only solid compound that can precipitate upon olivine dissolution. Literature highlights the co-precipitation of amorphous silica ($SiO_{2(am)}$) and iron-oxides (Giammar et al., 2005; Béarat et al., 2006). Both are suspected to precipitate mainly on the Mg-depleted olivine surface. These solids can be modeled in the same way as described above for magnesite. However, empirical kinetic parameters are

lacking, and therefore a higher level of details is not justified. In this work, a PBE and mass balance was only formulated for amorphous silica and concentration of total silicon in solution, respectively. Silicon as a linking component in olivine is expected to play an important role when fitting the model to data from carbonation experiments. As a starting point, the rate law for surface nucleation (Eq. (37)) was chosen and the parameters k_s and K_s were adopted from the magnesite precipitation.

2.4. Geochemical model

Geochemical software package EQ3/6

The software package EQ3/6 V8.0 (Wolery, 1992) was used for to run geochemical simulations. Given the temperature, CO_2 pressure and solution composition the supersaturation ratio with respect to magnesite, amorphous silica and other possible precipitates, as well as the formation of complexes and the pH were calculated. However, such a package leads to a manifold increase in computational time, if run together with the Matlab ode15s solver.

Reduced set of reactions

To overcome this constraint, a reduced set of reactions has been formulated, covering the species of major relevance. Listed in Table 2-2 are the species and reactions considered for the H_2O-CO_2-olivine system.

Table 2-2: Relevant species and reduced set of reactions for the H_2O-CO_2-olivine system.

10 species in solution	
$CO_{2(aq)} - HCO_3^- - CO_3^{2-} - H^+ - OH^- - Mg^{2+} - Si(OH)_4^{\circ\,a)} - SiO(OH)_3^- - MgHCO_3^+ - MgCO_{3(aq)}$	
set of 10 reactions	
(I)	$CO_{2(g)} \longleftrightarrow CO_{2(aq)}$
(II)	$CO_{2(aq)} + H_2O \longleftrightarrow HCO_3^- + H^+$
(III)	$HCO_3^- \longleftrightarrow CO_3^{2-} + H^+$
(IV)	$H_2O \longleftrightarrow OH^- + H^+$
(V)	$Mg_{1.82}Fe_{0.18}SiO_{4(s)} + 4H_2O \longrightarrow 1.82Mg^{2+} + 0.18Fe^{2+} + Si(OH)_4^{\circ} + 4OH^-$
(VI)	$MgCO_{3(s)} \longleftarrow Mg^{2+} + CO_3^{2-}$
(VII)	$SiO_{2(am)} + 2H_2O \longleftarrow Si(OH)_4^{\circ}$
(VIII)	$Si(OH)_4^{\circ} \longleftrightarrow SiO(OH)_3^- + H^+$
(IX)	$Mg^{2+} + HCO_3^- \longleftrightarrow MgHCO_3^+$
(X)	$Mg^{2+} + CO_3^{2-} \longleftrightarrow MgCO_{3(aq)}$
key to reactions	
(I) solubility of CO_2 in water; (II) dissociation of carbonic acid; (III) dissociation of bicarbonate; (IV) dissociation of water; (V) dissolution of olivine; (VI) precipitation of magnesite; (VII) precipitation of amorphous silica; (VIII) first dissociation of silicic acid; (IX) formation of the complex magnesium bicarbonate; (X) formation of the complex aqueous magnesite	

[a] The notations for aqueous silicon, $Si^{4+}_{(aq)}$, and silicic acid, $Si(OH)_4^{\circ}$, are treated as equivalents.

While the thus reduced geochemical model considers instantaneous equilibrium in solution, the solid phase reactions, i.e. dissolution and precipitation, are instead time-dependent. Moreover, the solubility equilibria (V) – (VII) are only applicable if the corresponding solid is still/already present. Additional relations would be needed in the case of their absence.

Mass balances for total Mg and Si in solution

Knowing the total magnesium and silicon in solution from the mass balances (Eq. (28)) renders a case differentiation unnecessary. The following two mass balances can readily be applied:

$$c_{Mg(aq)} = c_{Mg^{2+}} + c_{MgHCO_3^+} + c_{MgCO_{3(aq)}}, \tag{38}$$

$$c_{Si(aq)} = c_{Si(OH)_4^\circ} + c_{SiO(OH)_3^-}. \tag{39}$$

Thermodynamic data

Accepting the assumption of ideal solution, i.e. activity coefficients equal to 1, seven equilibrium relationships for reactions (I) – (IV) and (VIII) – (X) can be formulated via the corresponding equilibrium constants, K_i. Using the Van't Hoff equation, reactor temperatures apart from standard condition could be simulated:

$$K_i(T) = K_i^\circ \exp\left(\frac{-\Delta H_r^\circ}{R}\left(\frac{1}{T} - \frac{1}{T^\circ}\right)\right). \tag{40}$$

Table 2-3 reports the thermodynamic data needed, i.e. the standard enthalpy of reaction $\Delta H_r°$, the standard Gibbs free energy $\Delta G_r°$ and the standard equilibrium constant $K°$ (at T° = 298.15°K). This data has been calculated based on the energies of formation that are listed in the CODATA database (Lide, 2007); exceptions are marked by index. Equilibrium constants were calculated from $\Delta G_r° = -RT° \ln K°$.

Table 2-3: List of thermodynamic data.

Reaction No°	$\Delta H_r°$ [kJ mol^{-1}]	$\Delta G_r°$ [kJ mol^{-1}]	$K°$ [–]
(I)	-19.75	8.4	$10^{-1.4717}$
(II)	9.16	36.3	$10^{-6.3598}$
(III)	14.70	59.0	$10^{-10.3369}$
(IV)	55.82	79.9	$10^{-13.9987}$
(VIII) [a)]	25.60	56.0	$10^{-9.8113}$
(IX) [b)]	3.30	-6.1	$10^{1.0705}$
(X) [c)]	11.35	-17.0	$10^{2.9784}$

[a)] energies of formation for all species of the reaction taken from Nordstrom and Munoz (1994)
[b)] $\Delta H/G_r°(MgHCO_3^+)$ taken from Nordstrom and Munoz (1994)
[c)] $\Delta H/G_r°(MgCO_{3(aq)})$ taken from Nordstrom and Munoz (1994)

Charge balance

Given the 10 unknown aqueous species as listed in Table 2-2, the two mass balances in Eqs. (38) and (39) and the 7 equilibria relationships provide only 9 equations. Writing the charge balance gives the missing 10th relation in order to solve the geochemical system:

$$2c_{Mg^{2+}} + c_{MgHCO_3^+} + c_{H^+} = c_{OH^-} + c_{HCO_3^-} + 2c_{CO_3^{2-}} + c_{SiO(OH)_3^-}. \quad (41)$$

The code for PBE and geochemical model is attached in Appendix 2.

2.5. Sensitivity analysis

Analyzed parameters

Using the reactor model and the simplified geochemical model as described above, a sensitivity analysis has been performed in order to elucidate the influence of:

1. temperature
2. CO_2 pressure
3. olivine particle size

Setting the reactor conditions

The carbonation of 30 g olivine particles in 170ml reactor solution was simulated. This corresponds to a solid-liquid ratio of 15%, the same ratio that was applied in the carbonation studies by O'Connor et al. at the Albany Research Center from 1999 till 2005 (e.g. O'Connor et al., 2004). Since the flow through of a CFSTR system exhibits a delaying effect on the degree of supersaturation, all simulations were run in batch mode. The operating condition of 120°C, 100bar CO_2 pressure and olivine size fraction from 90 – 180 μm were chosen as a reference that remained fixed while other parameters were varied.

Setting the shape factors

Sieving fractions of irregular but geometrically similar particles results in shape factor from 0.5 to 0.7 (Randolph and Larson, 1988). For the sake of simplicity, volumetric shape factors k_v were kept constant at $\pi/6$ for all solid compounds throughout the sensitivity analysis and the experimental part. This value corresponds to the shape factor of a sphere. The same factor is used to measure the 1-D particle volume distributions by electronic zone sensing instruments such as the Coulter Multisizer.

Setting the initial PSDs

In order to parameterize particle size, the mean of the mesh size of two sieves that are used to obtain a certain size fractions of olivine particles, $L°$, was used to calculate generalized PSDs. Commonly used to describe distributions of sieve fractions is the Rosin-Rammler (RR) distribution (Meersmann, 1995), whose probability density function (PDF) is given by:

$$f(L|k,L^\circ) = \frac{k}{L^\circ}\left(\frac{L}{L^\circ}\right)^{k-1} \exp\left(-\left(\frac{L}{L^\circ}\right)^k\right), \quad (42)$$

for $L > 0$, and $f(L|k,L°) = 0$ for $L \leq 0$. The dispersion parameter k was related to the position parameter $L°$ by taking the square root of the latter. Thus it was possible to simulate particle populations at any given mean particle size $L°$ consistently. For illustration, Appendix 3 shows the RR-PDFs related to the four different size fractions 0 – 37 μm, 37 – 90 μm, 90 – 180 μm and 180 – 355 μm. Also shown for comparison are corresponding Gaussian PDFs, calculated using $L°$ and $k = (L°)^{0.5}$ as the mean and variance of the normal distribution.

Setting the specific surface area

To estimate the total particle surface area that corresponds to a given $L°$, a set of BET measurements for different size fractions between 0 and 355 μm was taken from literature (O'Connor et al., 2004; Hänchen et al., 2007). By applying a logarithmic regression, the following correlation was found:

$$a_{BET} = -0.1527\ln(L°) - 1.2049. \quad (43)$$

The data for Eq. (43) is attached in Appendix 4.

Quantitative sensitivity measure

The amount of CO_2 that is sequestered in magnesite within a 3 h simulation, m_{CO2} (mol), was taken as the measure to quantify model sensitivity. For each parameter, p_i (i=1,2,3; see p. 12), a series of base values was defined and subsequently varied by ± 5% before running the simulations again. The other parameters remained fixed at the reference conditions defined above. The model sensitivity, s, was calculated using the differential quotient given by (Saltelli et al. 2000):

$$s_i = \frac{\Delta m_{CO_2}}{\Delta p_i^{\pm 5\%}} \quad (i=1,2,3), \quad (44)$$

which corresponds to the discretized partial derivative of the sequestered CO_2 with respect to temperature, CO_2 pressure and particle size. The results are shown in Figs. 2-1 to 2-3.

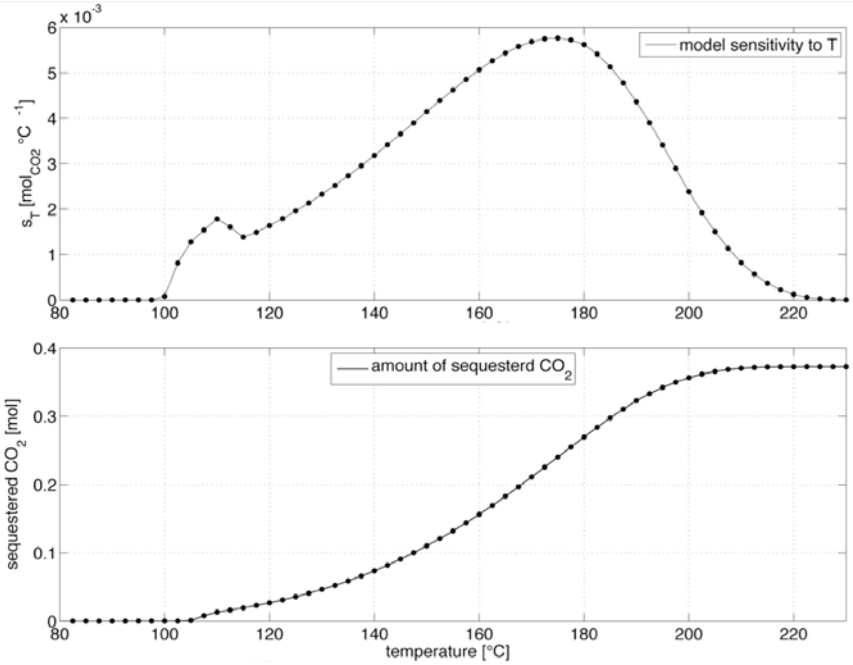

Figure 2-1: Carbonation of the 90 – 180 μm size fraction at P_{CO2} = 100 bar; model sensitivity to a ± 5% perturbation of temperature (a) and amount of CO_2 sequestered within a 3 h simulation (b); solid lines support visibility and are not a fit.

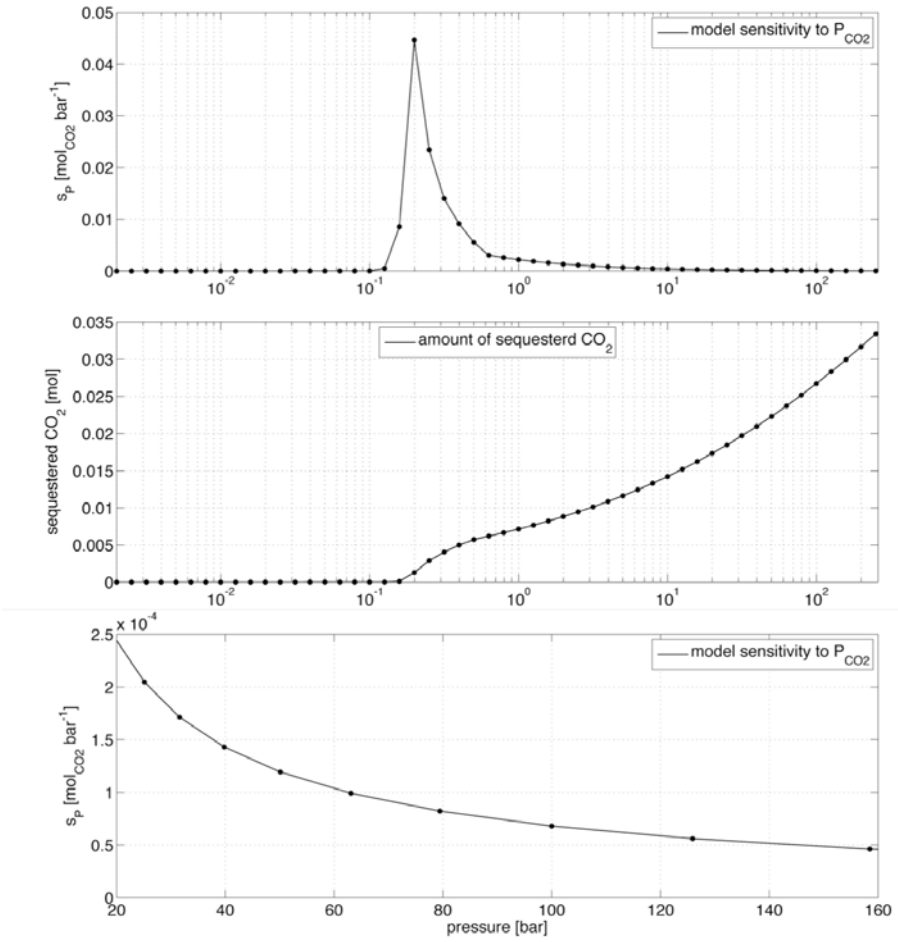

Figure 2-2: Carbonation of the 90 – 180 µm size fraction at T = 120°C; model sensitivity to a ± 5% perturbation of pressure (a), amount of CO_2 sequestered within a 3 h simulation (b), and an outtake of subplot (a), showing a pressure range as applied in praxis (c); x-axis in (a) and (b) are in logarithmic scale, solid lines support visibility and are not a fit.

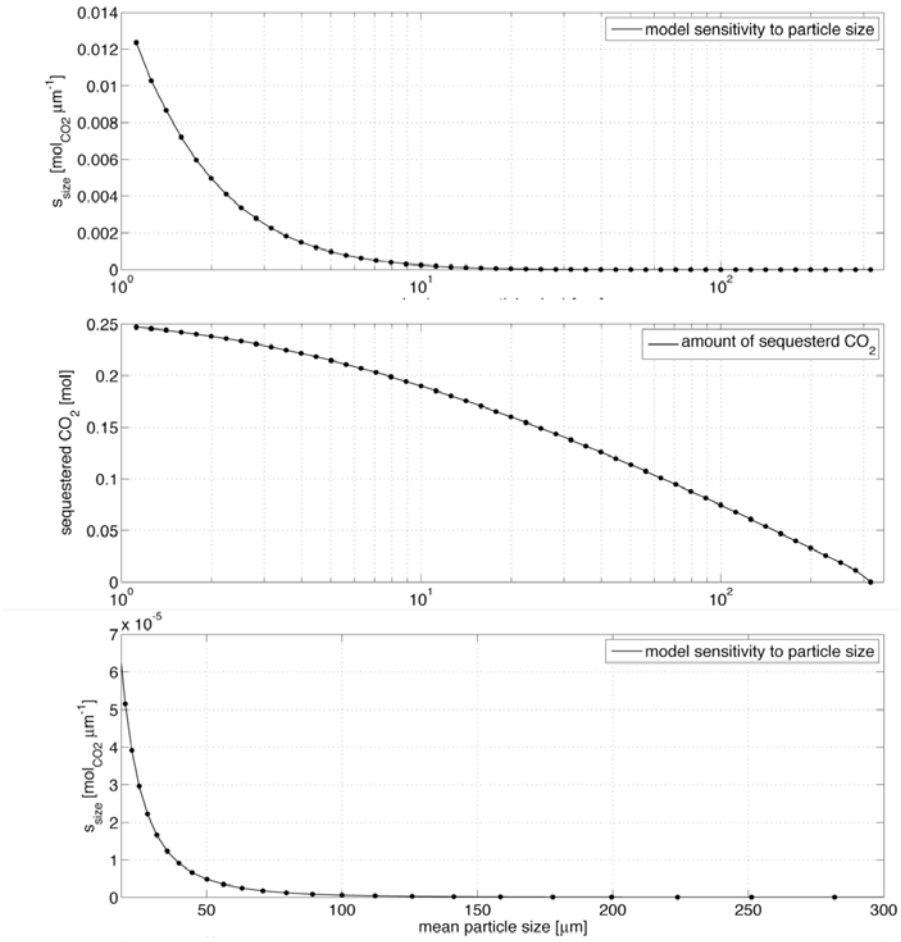

Figure 2-3: Carbonation at T = 120°C and P_{CO2} = 100 bar; model sensitivity to a ± 5% perturbation of mean particle size (a), amount of CO_2 sequestered within a 3 h simulation (b), and an outtake of subplot (a), showing the particle size range as applied in praxis (c); x-axis in (a) and (b) are in logarithmic scale, solid lines support visibility and are not a fit.

Model sensitivity: Conclusions

From this analysis, it results that the model is most sensitive to temperature between 170 and 180°C, while the sensitivity decreases towards the minimum temperature needed for magnesite precipitation to take place (at 100°C) and the one that is sufficient to convert all magnesium from the olivine to magnesite (at 220°C). The local maximum around 110°C is partly an artifact, owing to limited numerical precision at $\lim(m_{CO2}(p_i))=0$. The same local maximum can be observed in Fig. 2-2; the model sensitivity to CO_2 pressure is high only within the impractical range of 0.1 – 1 bar, below which magnesite does not precipitate. Instead, the scale of the y-axis in Fig. 2-2, subplot (c), reveals a minor perturbation effect for pressures that are reasonable for sufficiently fast magnesium conversion. This is due to the counteractive influence of the CO_2 pressure on the pH (low pH and thus better dissolution of olivine at high P_{CO2}) and on the availability of carbonate (more carbon in solution at high P_{CO2}, but most of it is present in a protonated form).

As expected, model sensitivity to particle size becomes high towards very fine particles. It is remarkable that even down to the minimum particle size examined, i.e. 1.1 μm, the operating conditions of 120°C and 100 bar P_{CO_2} are still too mild to carbonate all magnesium in the system. In practical, the mechanical pretreatment needed to achieve such fine particles would be extremely costly (O'Connor et al., 2005). Within the more applicable size range from 18 to 300 μm, as seen in Fig. 2-3, subplot (c), the model is two orders of magnitude less sensitive to particle size than to temperature. It follows that with the model developed the key parameter for controlling the extent of CO_2 conversion by mineral carbonation is the reactor temperature.

Non-quantitative representation of the model sensitivity

A non-quantitative representation of model sensitivity is given in Figs. 2-4 to 2-6, where the concentration developing of olivine, total magnesium in solution and magnesite illustrate the overall mineral carbonation process. Shown are four runs per plot, with temperature being set to 100, 120, 150, and 185°C, CO_2 pressure to 1, 50, 100, and 150 bar and the olivine particle size to the four distributions in Appendix 3 where L^* is equal to 18.5, 63.5, 135, and 267.5 μm, respectively. For the sake of a better distinguishability amongst the four runs, the initial olivine feed mass was reduced to 5 g, whereas the simulated time was increased to 6 h.

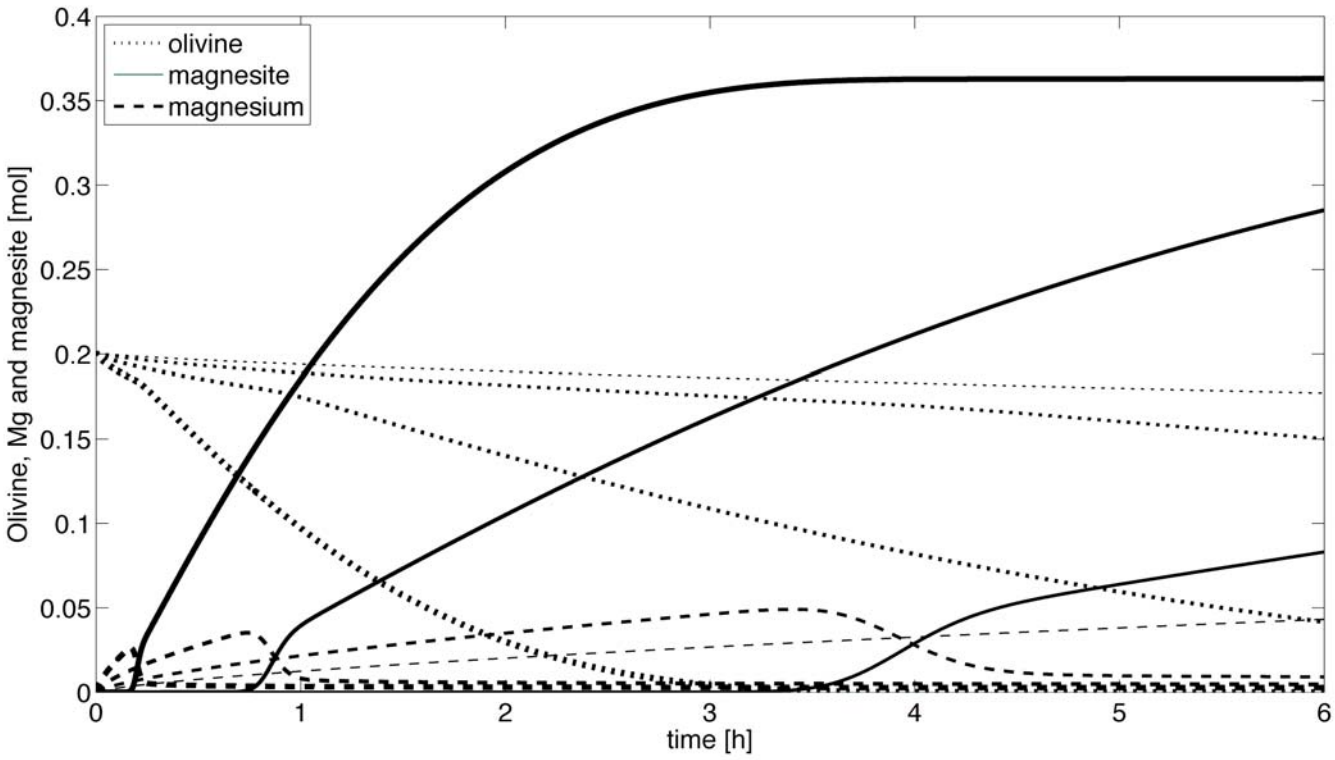

Figure 2-4: Effect of temperature on the mineral carbonation process; amount of olivine, total magnesium in solution and magnesite over time, see text for specification of operating conditions. Solid, dashed, and dotted lines represent magnesite, total magnesium in solution, and olivine, respectively. The thicker the lines, the higher the temperature.

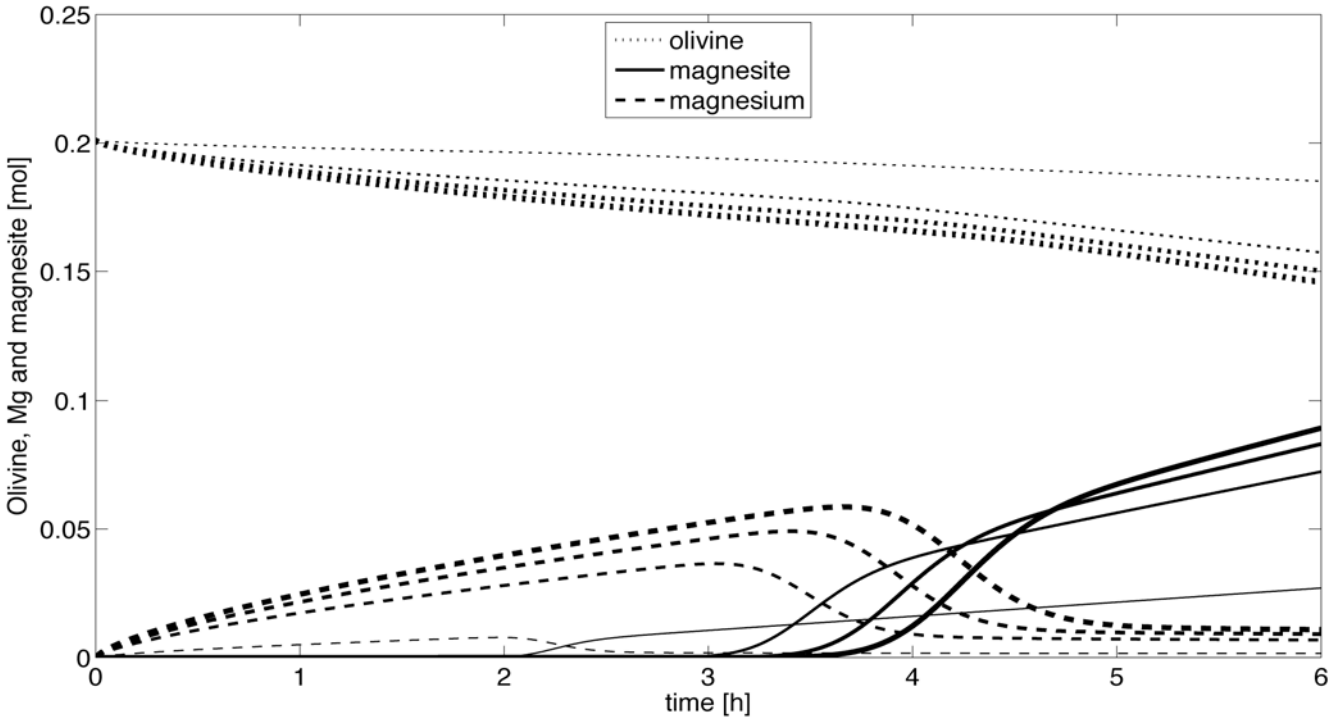

Figure 2-5: Effect of CO_2 pressure on the mineral carbonation process; amount of olivine, total magnesium in solution and magnesite over time, see text for specification of operating conditions. Solid, dashed, and dotted lines represent magnesite, total magnesium in solution, and olivine, respectively. The thicker the lines, the higher the CO_2 pressure .

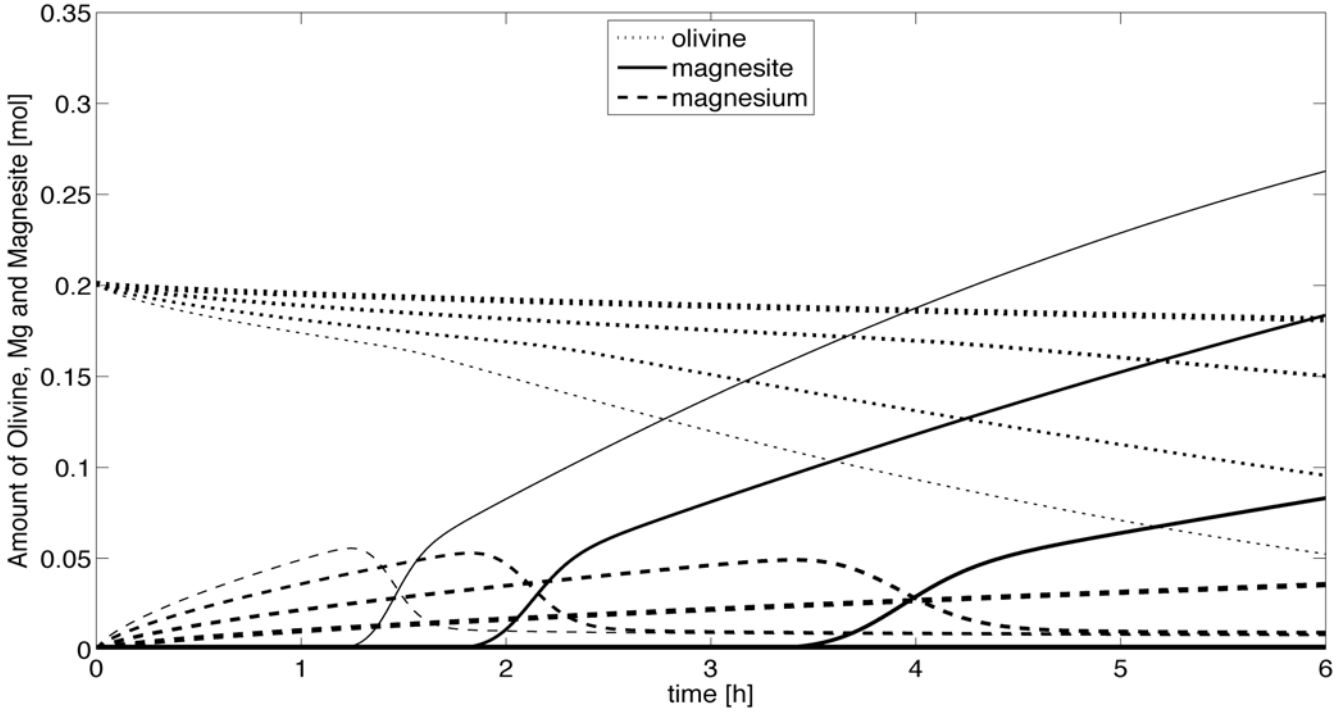

Figure 2-6: Effect of olivine particle size on the mineral carbonation process; amount of olivine, total magnesium in solution and magnesite over time, see text for specification of operating conditions. Solid, dashed, and dotted lines represent magnesite, total magnesium in solution, and olivine, respectively. The thicker the lines, the bigger the particle size.

Non-quantitative model sensitivity: Conclusions

Figs. 2-4 to 2-6 underline the conclusions drawn above regarding the strong model response to temperature above 100°C, the minor sensitivity to a change and the relative importance of particle size. Both a reduction of temperature and an increase in particle size substantially delay the time for magnesite precipitation to start. Fig. 2-5 shows that this is not the case for a rise in CO_2 pressure. The amount of sequestered CO2 can be slightly increased if increasing the P_{CO_2} but it takes longer to reach the onset of magnesite precipitation.

3. Materials and methods

3.1. Experimental set-up

San Carlos olivine

For previous studies within the same working group, gem-quality San Carlos olivine has been crushed, sieved and ultrasonically cleaned from adhering fines. The average chemical composition of the olivine was measured at $Mg_{1.82}Fe_{0.18}SiO_4$, giving a molar weight of 146.4 g mol^{-1} (electron microprobe analysis). The pretreated size fraction between 90 and 180 μm was chosen for the experimental part of this work. Its particle volume distribution has been measured using a Beckman Coulter Multisizer 3 in a 0.17 M NaCl solution; results were averaged over two to five measurements. The calculations for the transformation of the particle volume to the particle size distribution are described elsewhere (Hänchen et al., 2007). The specific surface of this fraction was measured at 797 ± 55 $cm^2\ g^{-1}$ (BET method, nitrogen adsorption).

Experimental set-up

Carbonation experiments were carried out in a stirred 300 ml titanium (grade 2) flow-through reactor, placed in an oil bath. Temperature was monitored with an in-situ thermometer, being connected to the oil bath for external temperature regulation. Flow-through was maintained by two HPLC pumps running at a concerted pump rate of Q = 1.15 ml min^{-1}. Setting Q to the minimum pump rate applicable with the pumps employed enabled to reach high magnesium concentrations in carbonation experiments without consuming big amounts of feed olivine[1]. Prior to the reactor inlet, a pre-heater was installed and run at 90°C, in order to minimize the thermal difference between feed and reactor solution. The outlet flow was cooled down to ambient temperature by a heat exchanger, filtered in-line through a 2 μm filter before being depressurized to ambient pressure via back-pressure regulator. The feed solution consisted of Millipore H_2O, which was purged overnight from oxygen and other atmospheric components with nitrogen (grade 5.0, 99.999% pure) prior to each experiment. The reactor was operated with 170 ml solution, the remaining volume containing the CO_2 atmosphere (grade 3.0, 99.9% pure). In order to maintain a constant gas pressure, the CO_2 was first compressed and confined in a high-pressure buffer tank before feeding it into the reactor via a front pressure regulator. Pressure was monitored both digitally and analogue. Fig. 3-1 shows the scheme of the experimental set-up.

[1] For a given dissolution rate, r, the magnesium concentration at equilibrium is controlled by the ratio between Q and initial olivine mass, $m_{O,d}$:

$$r = c_{Mg^{2+}}^{eq.} \frac{Q}{A_{BET} m_{0,d}}$$

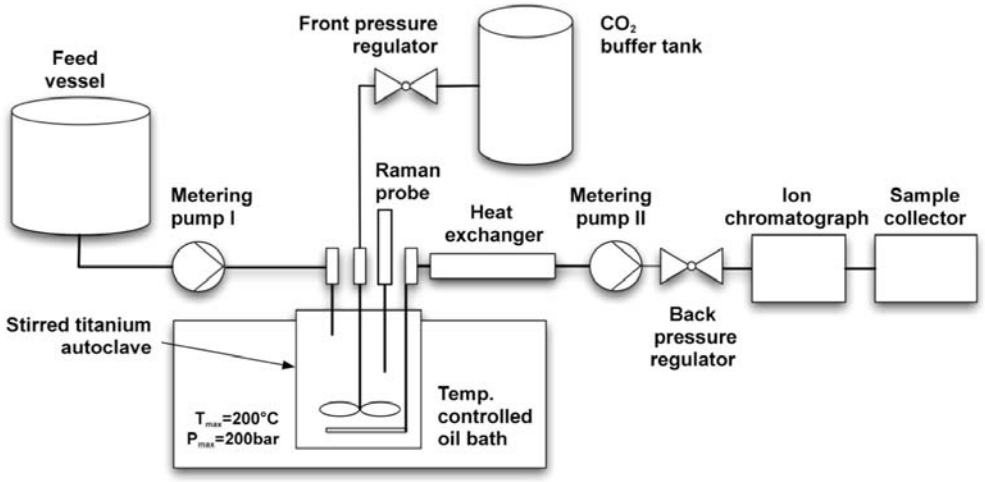

Figure 3-1: Scheme of the experimental set-up.

Stirrer testing: Particle suspension and heat transfer

Agitation was supplied by a gas-entraining four bladed titanium stirrer driven by a magnetic coupling in the reactor lid. The influence of the stirring rate on the effectiveness of particle suspension was tested using a 250 ml glass beaker, containing 170 ml H_2O and the maximum amount of olivine applied in the experiments. The reactor lid was installed atop of the beaker and the latter placed at the original distance between bottom and stirrer blades. Since the beaker had a 8% larger diameter than the reactor itself, it was guaranteed that the effectiveness of suspension is rather under- than overestimated. For documentation, the beaker was pictured from the side and below at each stirring rate.

A second test series should reveal the effect of stirring on the radial heat transfer inside the reactor under operating conditions. Therefore, the oil bath temperature was fixed at 140°C and the reactor temperature measured at different stirring rates. The data for both stirring test series is attached in Appendix 5.

Above a minimum rate of 600 rpm complete suspension of the particles was observed. Below 900 rpm, the funnel-shaped stirring vortex did not reach the beaker bottom and all internal parts that are supposed to stick into the liquid volume are well wetted. The effect of the stirring rate on the measured reactor temperature at fixed oil bath temperature was found to be negligible over a wide range of stirring rates. Based on these findings, stirring was kept constant at 700rpm throughout the experiments.

Teflon equipment

In order to prevent scaling of precipitates on metallic surfaces, a Teflon cover for the temperature probe, a Teflon container fitted to the inner dimensions of the titanium vessel and a stirrer made of Teflon was used. Covering the temperature probe was suspected to have an insulating effect, leading to a systematic underestimation of the true reactor temperature. Indeed, heating the reactor to 120°C and measuring temperature with and without the cover resulted in a difference of 2°C (see Appendix

6 for documentation). However, after each the test run with the Teflon equipment, reactor solution was found in the tiny space between container and reactor wall and between cover and probe. This was most likely due to the agitation and subsequent capillary forces. Since the conditions at such locations with a temperature and concentration regime different than in the bulk solution are not controllable, the decision was taken to omit the Teflon equipment.

Problems with the inlet pump

During the course of the experimental series, the inlet HPLC pump had to be exchanged, owing to its increasing inaccuracy in providing a constant flow against high backpressure during long experiments. The consequence was a reduction of the liquid level in the reactor, in an extreme case down to the level of the outlet tube. Since concentrations were the measured quantity, any results obtained with the defective pump had to be put in question and excluded.

3.2. Experimental procedure and analytical methods

Prior to an experiment

All experiments were carried out at operating conditions of 120°C and 100 bar of CO_2 pressure. To exclude the presence of oxygen, the reactor was purged with CO_2 5 times up to 10 bar, before filling it with Millipore H_2O using the inlet pump. After heating up, pressurizing and waiting for temperature and pressure to stabilize, the system was switched to continuous mode, which marked the begin of an experiment.

In-situ, in-line and off-line analytical methods

The first two carbonation experiments were monitored using Raman spectroscopy (Mettler-Toledo, model RA 400), in order to verify the time needed for the system to equilibrate and to detect the onset of precipitation. However, precipitates were below the detection limit in both runs, and for further experiments this method was omitted. The magnesium (Mg) concentration in the outlet solution was measured in-line at 10 min intervals using an ion chromatograph (CS12A column, Dionex). Samples were taken by an automatic fraction collector and stored in 10ml tubes for off-line measuring. If magnesium concentrations were expected to exceed 2 mM, samples were diluted prior to analysis and measured off-line. Silicon (Si) and iron (Fe) concentrations were measured spectrophotometrically using the Molybdate Blue method for silicon and the 5-sulfosalicyclic acid method for iron, respectively. Prior to the analysis, samples for iron analysis were acidified using nitric acid (HNO_3, 2 M), heated up and the pH fixed to 0.945 by addition of sodium hydroxide (NaOH, 3 M). Thus, the brownish precipitates that form due to the presence of oxygen at ambient condition were solubilized.

Analysis of the reacted particles

At the end of each experiment, the reactor was cooled down and depressurized in batch mode. The reactor solution was filtered, the collected solids were washed with Millipore H_2O, dried over night at room temperature and prepared to take scanning electron microscope (SEM) images (Zeiss, model LEO 1530). One experiment was carried out at a stirring rate of 50 rpm only. After this run, the reactor was opened, drained using a syringe and the solids were left untouched in the reactor over night

for drying. Additionally with this experiment, SEM-energy-dispersive x-ray spectroscopy (SEM-EDX) analysis was performed (FEI, model Quanta 200FEG).

ICP-OES analysis

During the experimental series, the ion chromatograph suddenly measured a highly irregular base line. The reason for this was a found to be a deficient eluent flow, which was caused either by maladjustment due to a defective display indication or by a offset of the eluent pump. The problem was solved finding the right adjustment of the pump manually, i.e. seeking the set point corresponding to a flow of 1.2 ml s^{-1}, which is the ideal value to run the device. This troubleshooting gave the occasion to test another analytical method, the inductively coupled plasma optical emission spectrometry (ICP-OES). Its ability to measure concentrations of any given metallic species simultaneously should open room of improvement compared to the time intensive threefold analysis for Si, Fe and Mg when measured off-line. Five samples of one experiment were acidified as described above for Fe analysis and further diluted by factor 100. ICP-OES standards were available for magnesium and iron, but no measurements for silicon could be carried out (Varian, model Vista-MPX).

EQ3/6

As aforementioned in the modeling part, the geochemical software package EQ3/6 has been used to calculate the pH, formation of complexes and supersaturation ratios under operating conditions. The package estimates aqueous activity coefficients using a database that employs an extended Debye-Hückel equation. The fugacity of CO_2 is needed as an input parameter and was calculated with the correlation presented by Wolf et al. (2004). EQ3/6 outputs were used to compare model simulations and to learn about possible precipitates.

4. Results and discussion

Carbonation experiments in batch

Initially, two carbonation experiments, numbered C1 and C2, were carried out in batch mode, as listed in Table 4-1. The solid-liquid ratio, *w*, was aimed at 5% as a starting point.

Table 4-1: Experimental conditions for carbonation experiments in batch system.

experiment	m_o [mg]	w_o [%]	T [°C]	P_{CO2} [bar]	Q [ml min^{-1}]	stirring [rpm]	duration [h min]	SEM
C1	8327.0	4.67	120.7	99.3	0	700	20 h 56'	no
C2	8327.5	4.67	121.0	100.9	0	700	18 h 7'	yes

EQ3/6 simulation for experiment C1

No precipitation of magnesium carbonates was detected by Raman spectroscopy during experiment C1. The difference in weight between initial olivine mass and filtrate was measured to be 617 mg (4.21 mM). This amount was used to run a simulation with EQ3/6 (equilibrium upon complete dissolution). According to the output, the pH reached a value of 5.4, up to 45% of the magnesium was trapped in complexes and the solution was supersaturated with respect to the solids listed in Table 4-2:

Table 4-2: Possible precipitates formed during carbonation experiment No° C1, EQ3/6 simulation.

solid compound	chemical formula	supersaturation *S*
hematite	Fe_2O_3	115'073.00
goethite	FeO(OH)	10'300.00
magnesioferrite	$MgFe_2O_4$	581.50
cronstedtite-7A	$MgFe(II)_2Fe(III)_2SiO_5(OH)_4$	190.90
iron(III)-hydroxide	$Fe(OH)_3$	88.30
quartz	$SiO_{2(cc)}$	18.00
magnesite	$MgCO_3$	7.29
α-cristobalite	$SiO_{2(\alpha\text{-cr.})}$	7.20
minnesotaite	$Fe_3Si_2O_5(OH)_4$	5.54
amorphous silica	$SiO_{2(am)}$	3.06
talc	$Mg_3Si_4O_{10}(OH)_2$	2.96
greenalite	$Fe_3Si_2O_5(OH)_4$	2.93
sepiolite	$Mg_4Si_6O_{15}(OH)_2{:}6H_2O$	1.24

Possible precipitation

The precipitation of iron oxides and/or hydroxides was confirmed on a macroscopic scale by a change in color from pale green for unreacted olivine to orange-brown for reacted material. Silica would be expected to precipitate in the form of quartz, but not in its amorphous form as reported in literature. The solution was fairly oversaturated with respect to magnesite. Instead, magnesioferrite would lower the availability of magnesium for mineral carbonation if its precipitation were confirmed. Up to

date, literature does not provide information about this issue. Magnesioferrite is mainly studied in material science where it is synthesized at much higher temperatures than applied here.

Carbonation experiment C2

During the second experiment in batch mode, C2, five samples of approximately 12 ml were taken via the outlet tubing and measured off-line using the IC. Shown in Fig. 4-1 are the experimental results, compared with the model predicition. While for a first run precipitation of magnesite was allowed, the nucleation rate *J* was set to zero for a second.

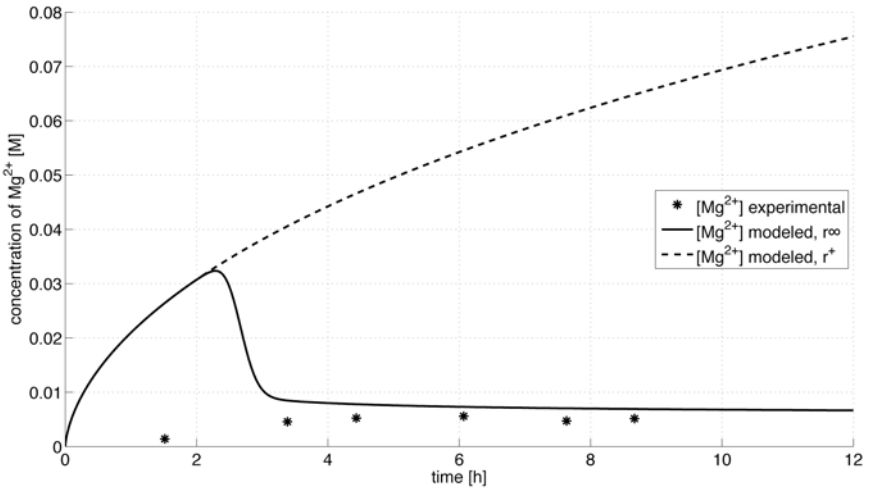

Figure 4-1: Concentration of Mg^{2+} over time from experiment C2, 18 h 7 min in batch mode with m_0 = 8327 mg; solid lines represent modeled concentrations at measuring conditions (25°C, ambient P_{CO2}).

Precipitation on the surface of reacted particles

Although the reactor solution was not replenished, concentration stabilized towards the middle of the experiment. The bulk reacted material was again of an orange-brownish appearance. However, also during this run possible precipitates were below the detection limit for in-situ Raman monitoring. Upon filtering the reacted particles, SEM images were taken. Thus, the formation of a fine-grained secondary phase on the olivine surface was visually confirmed, as shown in Fig. 4-2. For comparison, SEM images of unreacted olivine of the same size fraction are presented in the first two subplots.

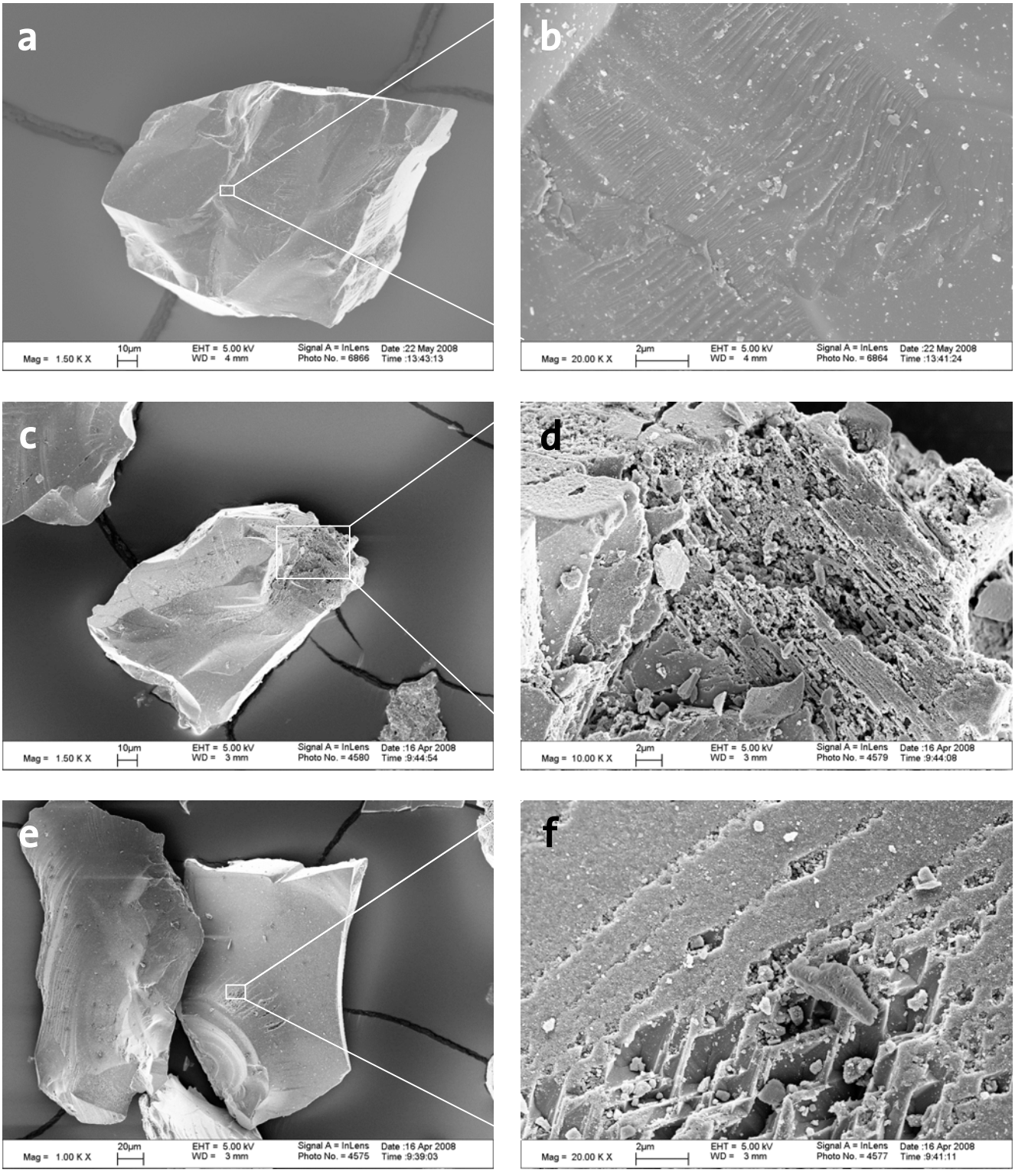

Figure 4-2: SEM images of unreacted (a, b) and reacted olivine from experiment C2 (c, d, e, f), 18 h 7 min in batch mode with m_o = 8327 mg.

Reasoning for discrepancy btw. measured and modeled Mg concentration

Three reasons can account for the poor model prediction of the measured concentration profile. Firstly, the dissolution rate proposed by Hänchen et al. (2006/2007) does not apply in general. Secondly, olivine dissolution was hindered by the formation and growth of the coarse coating observed by SEM analysis. This would imply that the kinetics in Eq. (32) do not apply in the carbonation experiment performed, where the initial amount of olivine was two orders of magnitude higher than Hänchen et al. (2006/2007) had used for their dissolution experiments. Thirdly, the coating contains magnesium-bearing solids that precipitate at much lower Mg^{2+} concentration than assumed in the model to be needed for nucleation and growth of magnesite.

Dissolution experiments in CFSTR

To test the first hypothesis, the next experiments were aimed at much lower magnesium concentrations. Therefore, the amount of feed olivine was reduced and the reactor was run in CFSTR mode. Additionally, the data from an olivine dissolution experiment (Exp. No° R92) performed by Hänchen et al. (2007) was used to compare their experimental results with the model prediction of this work. During the course of this experimental series, the feed mass of olivine has been raised after each run, in order to find a threshold in the extent of dissolution, i.e. in the measured magnesium concentration, after which the general dissolution rate does not apply anymore. Table 4-3 lists the experimental conditions and specifications.

Table 4-3: Experimental conditions for dissolution experiments in CFSTR system.

experiment	m_o [mg]	w_o [%]	T [°C]	P_{CO2} [bar]	Q [ml min^{-1}]	stirring [rpm]	duration [h min]	SEM
R92	11.34	6.67e-2	120.7	101.6	1.87	700	4 h 56'	no
R137	36.20	2.12e-1	120.7	101.5	1.13	700	6 h 20'	no
R139	202.84	1.19	120.6	101.2	1.12	700	7 h 52'	yes
R143	750.97	4.40	120.5	100.2	1.15	50	6 h 18'	yes
R144	749.46	4.39	120.7	101.0	1.16	700	11 h 1'	yes
R145	7502.05	42.26	120.5	101.0	1.16	700	9 h 25'	yes

Confirming the validity of the dissolution rate

Figs. 4-3 and 4-4 illustrate that for the first two experiments at low initial olivine mass, R92 and R137, the model predictions are – within the error given for r – in very good agreement with the measured magnesium concentration. Shown are the experimental results and three simulations where the dissolution rate from Eq. (32) has been used in its general form and including the errors given for the rate of reaction, α, and the pre-exponential factor $\tilde{U}$; indicated as r^o, r^+, and r^-.

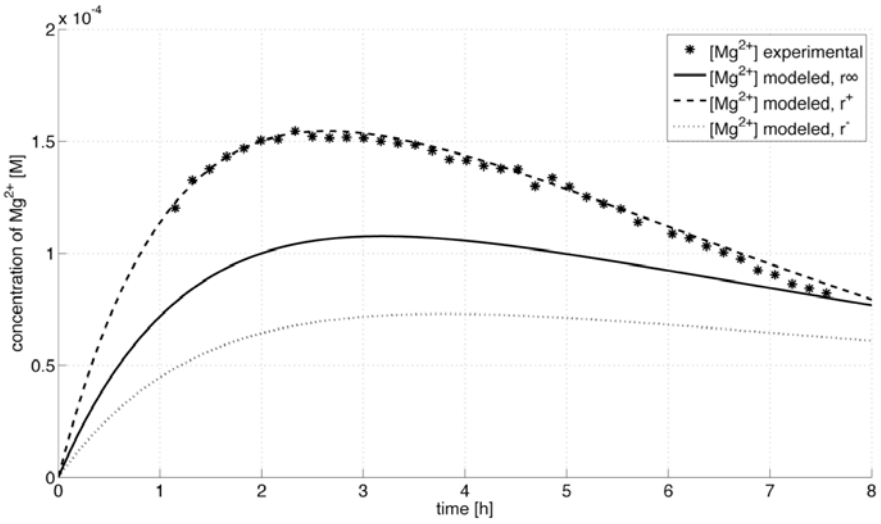

Figure 4-3: Concentration of Mg^{2+} over time from experiment R92 (Hänchen et al. 2007), 4 h 56 min in CFSTR mode with m_o = 11 mg; solid (r°), dashed (r^+), and dotted (r^-) lines represent modeled concentrations at measuring conditions (25°C, ambient P_{CO2}).

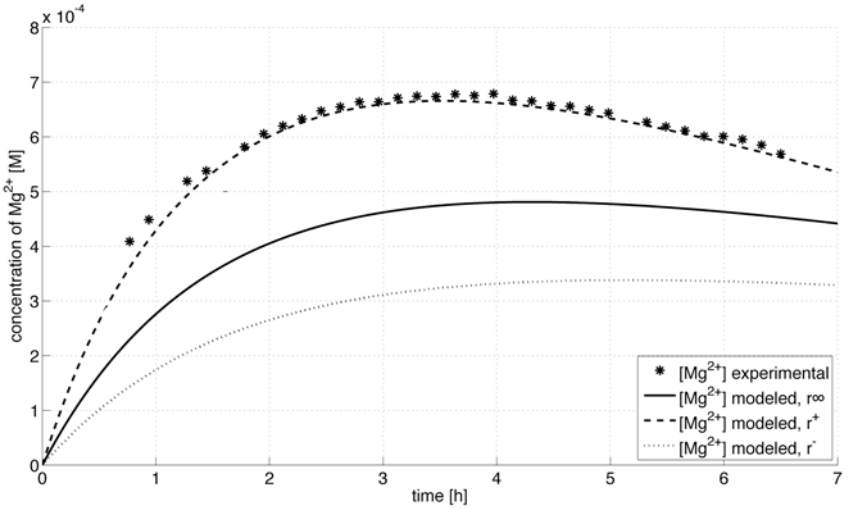

Figure 4-4: Concentration of Mg^{2+} over time from experiment R137, 6 h 20 min in CFSTR mode with m_o = 36 mg; solid (r°), dashed (r^+), and dotted (r^-) lines represent modeled concentrations at measuring conditions (25°C, ambient P_{CO2}).

Increasing the initial mass of olivine

Raising the initial olivine mass to 200 mg resulted in a leveling of the measured magnesium concentration around 1.3 mM, as shown in Fig. 4-5. The model failed to describe this shape properly, but the simulated concentrations still enclosed the measurements well. Fig. 4-6 illustrates the dissolution stoichiometry regarding Fe and Si release. Plotted are measured concentrations of both Fe and Si against the Mg-measurements. Solid lines indicate congruent dissolution.

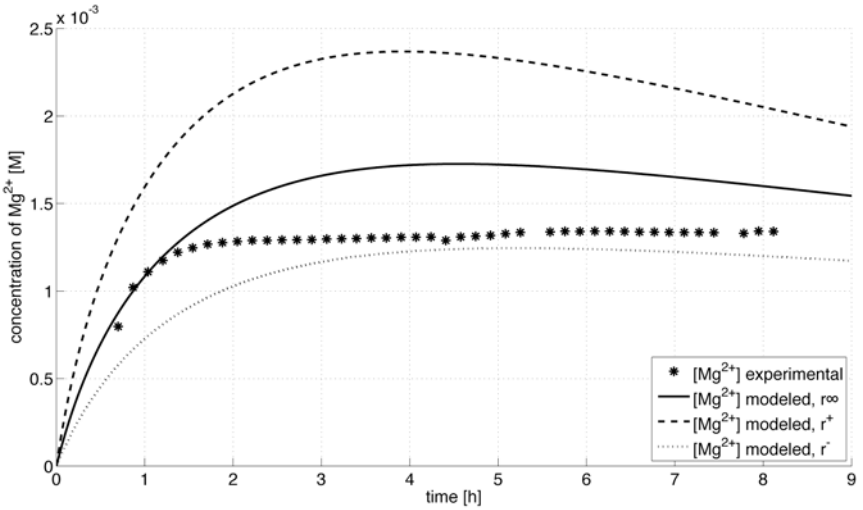

Figure 4-5: Concentration of Mg^{2+} over time from experiment R139, 7 h 52 min in CFSTR mode with m_o = 202 mg; solid (r°), dashed (r^+), and dotted (r^-) lines represent modeled concentrations at measuring conditions (25°C, ambient P_{CO2}).

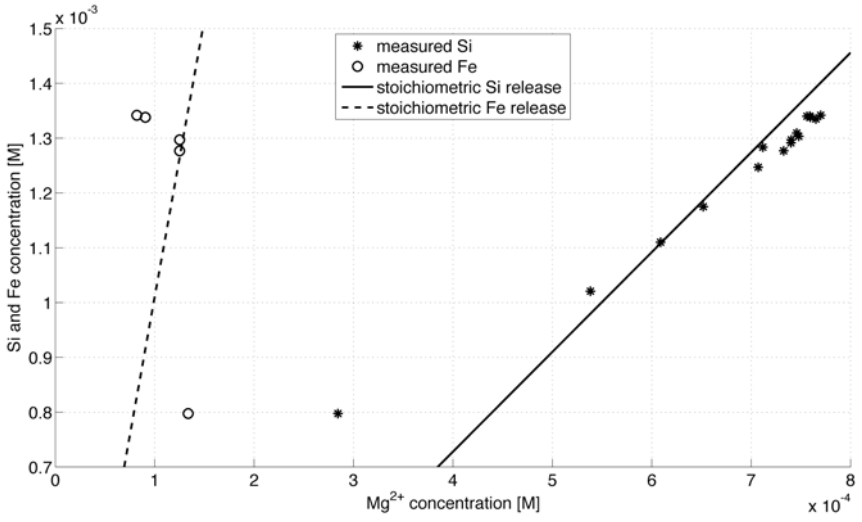

Figure 4-6: Measured concentrations of Fe and Si against Mg measurements for experiment R139, 7 h 52 min in CFSTR mode with m_o = 202 mg; solid and dashed lines represent stoichiometric release for Si and Fe, respectively.

Dissolution stoichiometry for experiment R139

At the beginning of the experiment, a preferential Fe and Mg release with respect to Si was measured. Towards the end, the Mg:Si ratio was slightly below the stoichiometric value. This suggests either a preferential Si release, which is unlikely according to the dissolution mechanism under acidic conditions, or a bias in the analytical methods (for Mg and/or Si). It could also indicate the removal of ionic Mg by precipitation of Mg bearing solids. The ratio Fe:Mg droped below the stoichiometric value, which is in good agreement with the EQ3/6 simulations that reveal very

high supersaturation ratios with respect to the iron-oxides listed in Table 4-2. Apparently the energy barrier for the precipitation process was overcome.

SEM image analysis for experiment R139

SEM images of the reacted particles showed evidence of advanced dissolution such as the formation of etch pits, whose shape and orientation depend on the crystallographic direction along which the crystal lattice broke during crushing (Awad et al., 2000). The formation of secondary phases was observable only on distinct parts of the particle surfaces, as seen in Fig. 4-7. This is most likely due to preferential precipitation on crystallographically suitable surfaces.

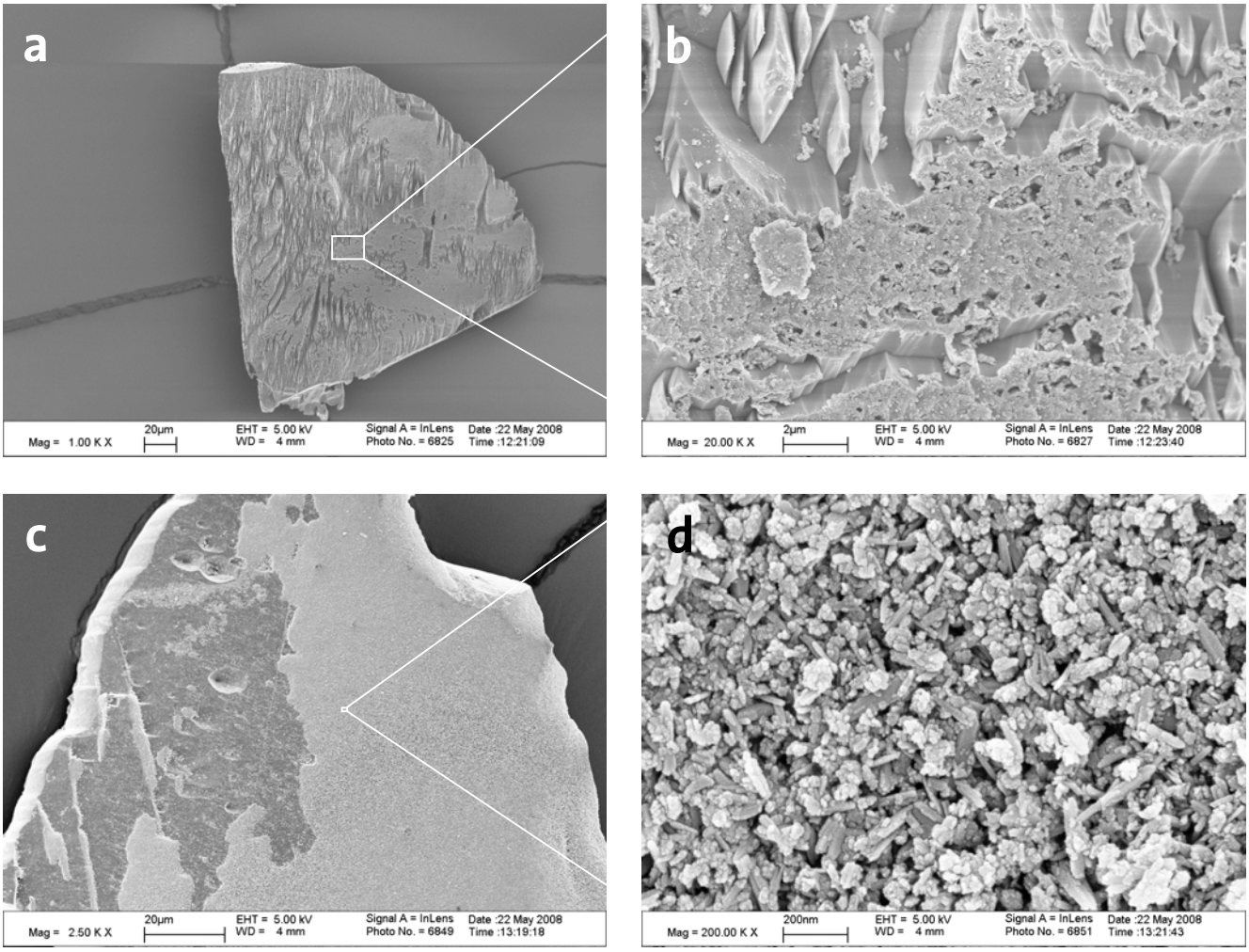

Figure 4-7: SEM images of reacted olivine from experiment R139, 7 h 52 min in CFSTR mode with m_o = 202 mg; for comparison with SEM images of unreacted olivine, see Fig. 4-2 on p. 25.

Producing single crystals

The formation of a fine-grained coating rather than single, freestanding crystals was attributed to the agitation by stirring, i.e. to particle-particle, particle-wall, and particle-stirrer interactions. In order to create locally unperturbed conditions with supersaturation ratios higher than in the bulk solution, the next experiment (R143) was carried out at a stirring rate that is insufficient to keep the particles in suspen-

sion. An initial mass of 750 mg of olivine and a stirring rate of 50 rpm was applied. SEM image analysis confirmed the formation of single solid phases, although the crystals did not grew bigger than a few microns; see Fig. 4-8.

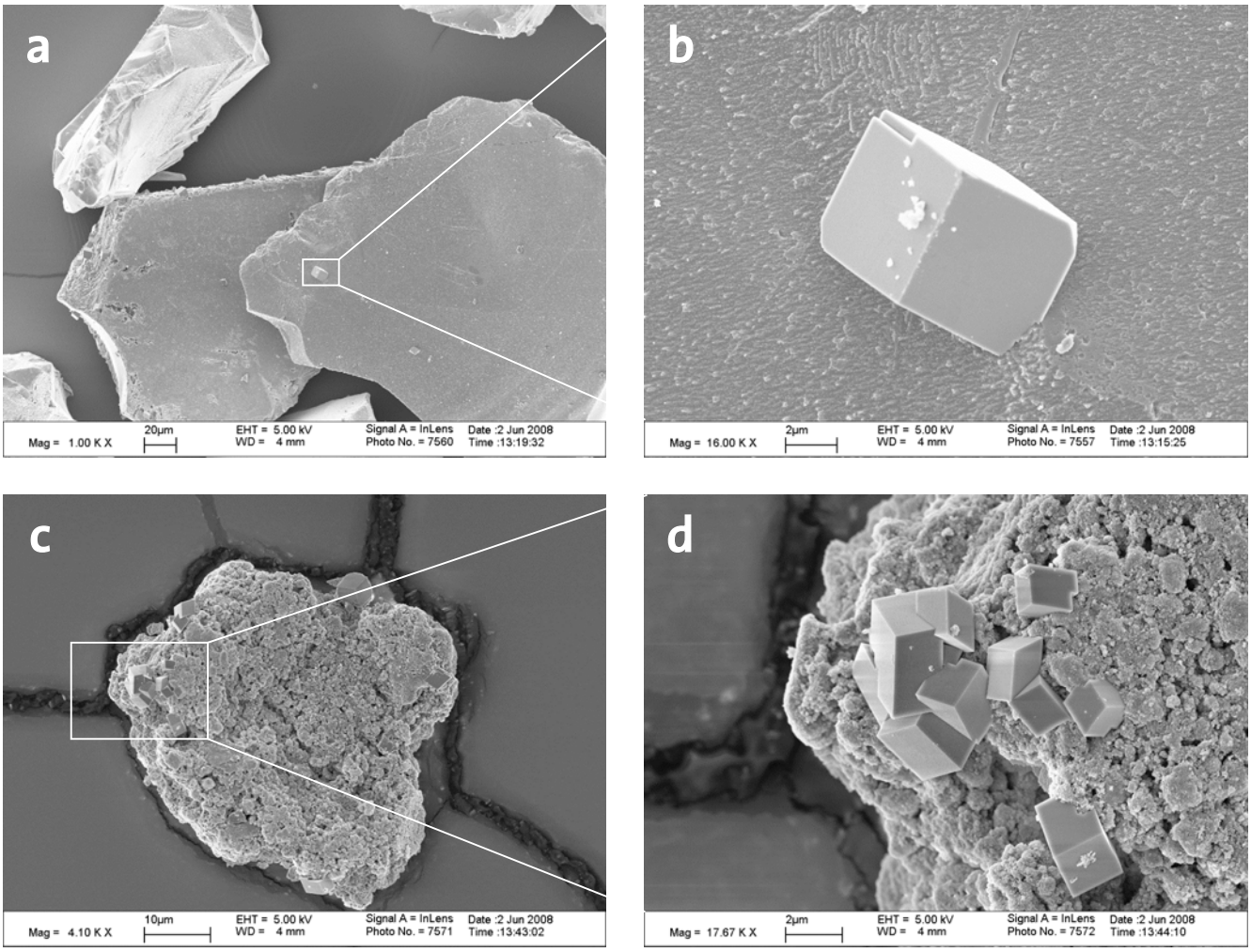

Figure 4-8: SEM images of reacted olivine from experiment R143, 6 h 18 min in CFSTR mode with m_o = 750 mg, stirring rate exceptionally at 50 rpm; for comparison with SEM images of unreacted olivine, see Fig. 4-2 on p. 25.

SEM-EDX analysis for experiment R143

In order to characterize the elemental composition of these precipitates, SEM-EDX analysis was performed. SEM-EDX works best with smooth, homogeneous surfaces of material that is thick enough to prevent the detection of background signals from underlying material. Both prerequisites were not satisfactorily fulfilled with the analyzed crystals. Since the detector had a minimal resolution of approximately 3 µm, the measurements did not allow for a conclusive identification. The EDX spectra of one of the bigger crystals found in the sample is shown in Fig. 4-9. For comparison, the spectra of an unaltered olivine surface from the feed size fraction is added.

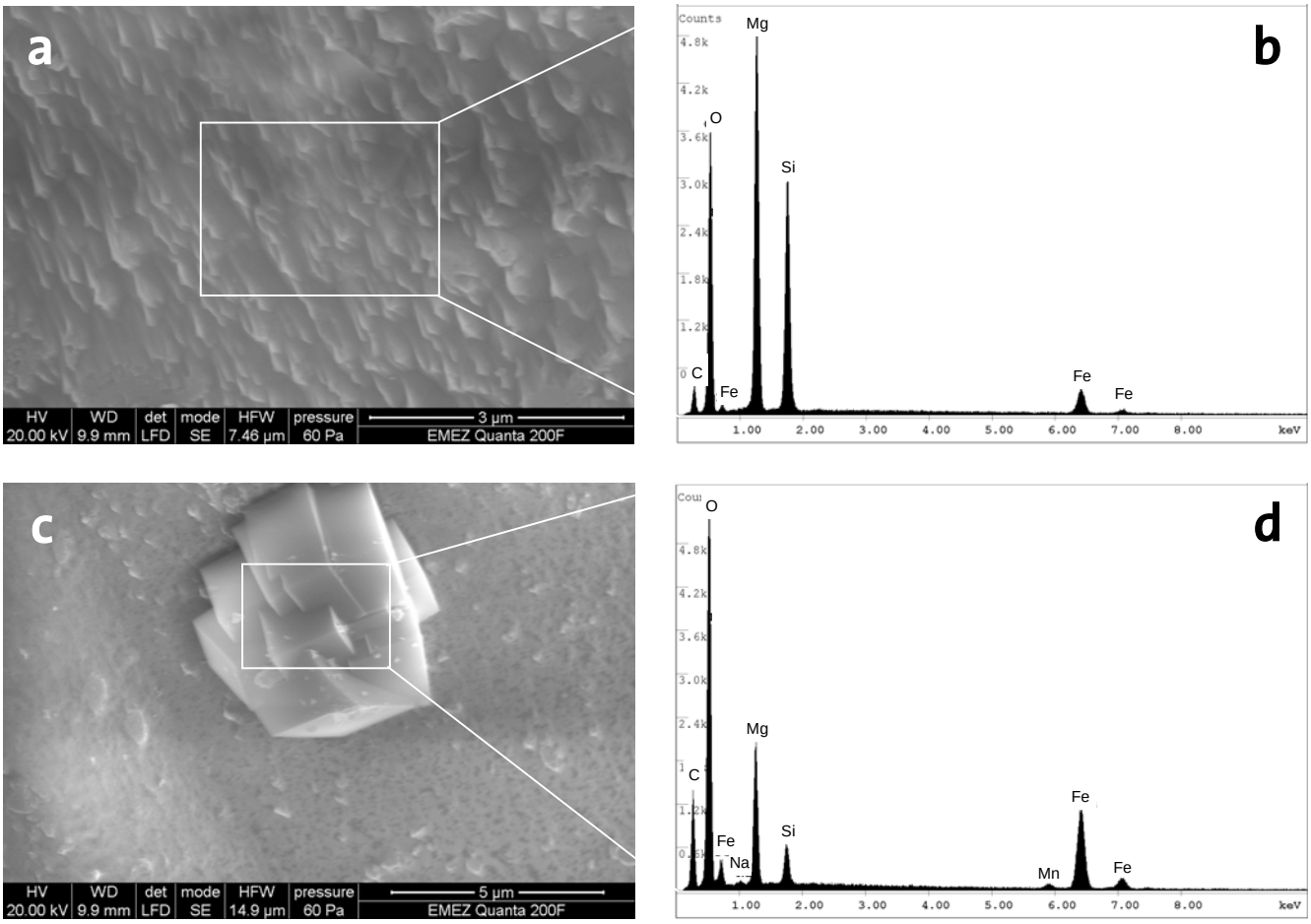

Figure 4-9: SEM images and EDX spectra of unreacted (a, b) and reacted olivine from experiment R143 (c, d), 6 h 18 min in CFSTR mode with m_o = 750 mg, stirring rate exceptionally at 50 rpm.

Results and discussion of SEM-EDX analysis

All elements in the H_2O-CO_2-olivine system have been detected with the electron beam centered on the single-phase crystals shown above. The signal intensity, i.e. the number of x-ray counts per element, may be interpreted only semi-quantitatively. The measured spectra in Fig. 4-9, subplot d and f, show enrichment in carbon, oxygen, and iron relative to unreacted olivine. The Mg- and Si-peaks were most likely caused by the background signal from the surrounding olivine, owing to the their similar proportion compared with the signal from fresh olivine. Sodium (Na) and manganese (Mn) appear as two small peaks. While the source of Na was found to be the Millipore H_2O used at that time, the reason for the presence of Mn remained unclear. The carbon peak in the spectra of the unreacted olivine is the result of sample coating for imaging.

Initially, the analyzed crystals were suspected to be magnesite. EDX spectra for magnesite found in literature differ substantially from the measurements presented above. Giammar et al. (2005) studied aqueous mineral carbonation for olivine at similar conditions as applied in this work. The Mg-peak in their spectra for magnesite

was higher than the one for O, while Fe and Si were completely absent. The spectra obtained here is very similar to the pattern measured by Giammar et al. (2005) for clusters of Fe-rich material that they found in the vicinity of etch pits on reacted olivine, but the exact composition was not further specified. As the crystals in Fig. 4-9 contain not only O and Fe, but also C, a logical identification would be iron carbonate (siderite, $FeCO_3$). According to simulations with EQ3/6, however, magnesite would precipitate much earlier than siderite under the conditions applied.
Increasing the initial olivine mass and prolonging the duration of an experiment should generate big enough crystals that allow for an unambiguous identification by SEM-EDX analysis.

Redo of experiment R143 at normal stirring rate

First, the same experiment was repeated applying the normal stirring rate of 700 rpm, in order to close the gap in the experimental course. The raise in mass up to 750 mg seemed to increase the deviation from the model prediction for the measured magnesium. However, already in this experiment (R144) the inlet pump became inaccurate. During this long run (11 h), the liquid volume in the reactor decreased from initially 170 to 140 ml. Consequently, the reactor solution became more concentrated with time. The measured concentration profile showed an upward trend throughout the experiment, which is unusual for a run in CFSTR mode. Fig. 4-10 shows the experimental data together with the modeled concentrations. Fig. 4-11 shows again distinct parts of the olivine surface being covered with a coarse coating similar to the observations in R139 and in the carbonation experiments.

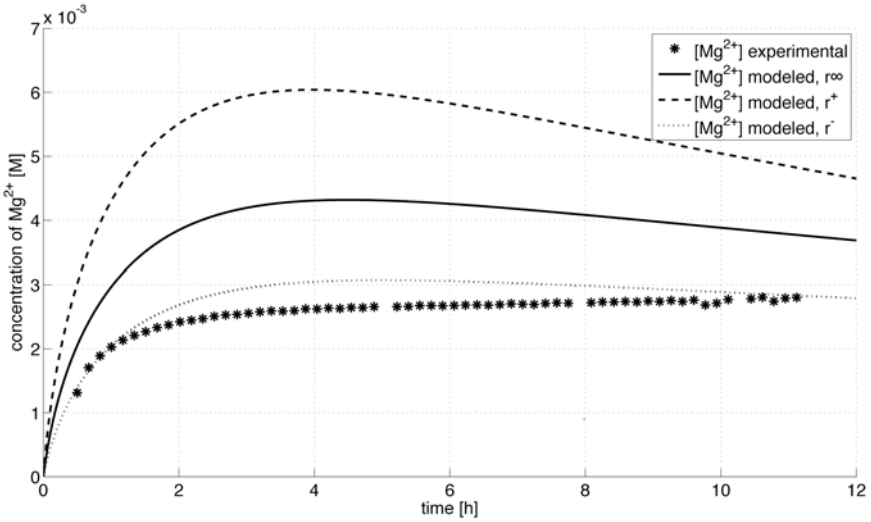

Figure 4-10: Concentration of Mg^{2+} over time from experiment R144, 11 h 1 min in CFSTR mode with m_o = 749 mg; solid (r^o), dashed (r^+), and dotted (r^-) lines represent modeled concentrations at measuring conditions (25°C, ambient P_{CO2}).

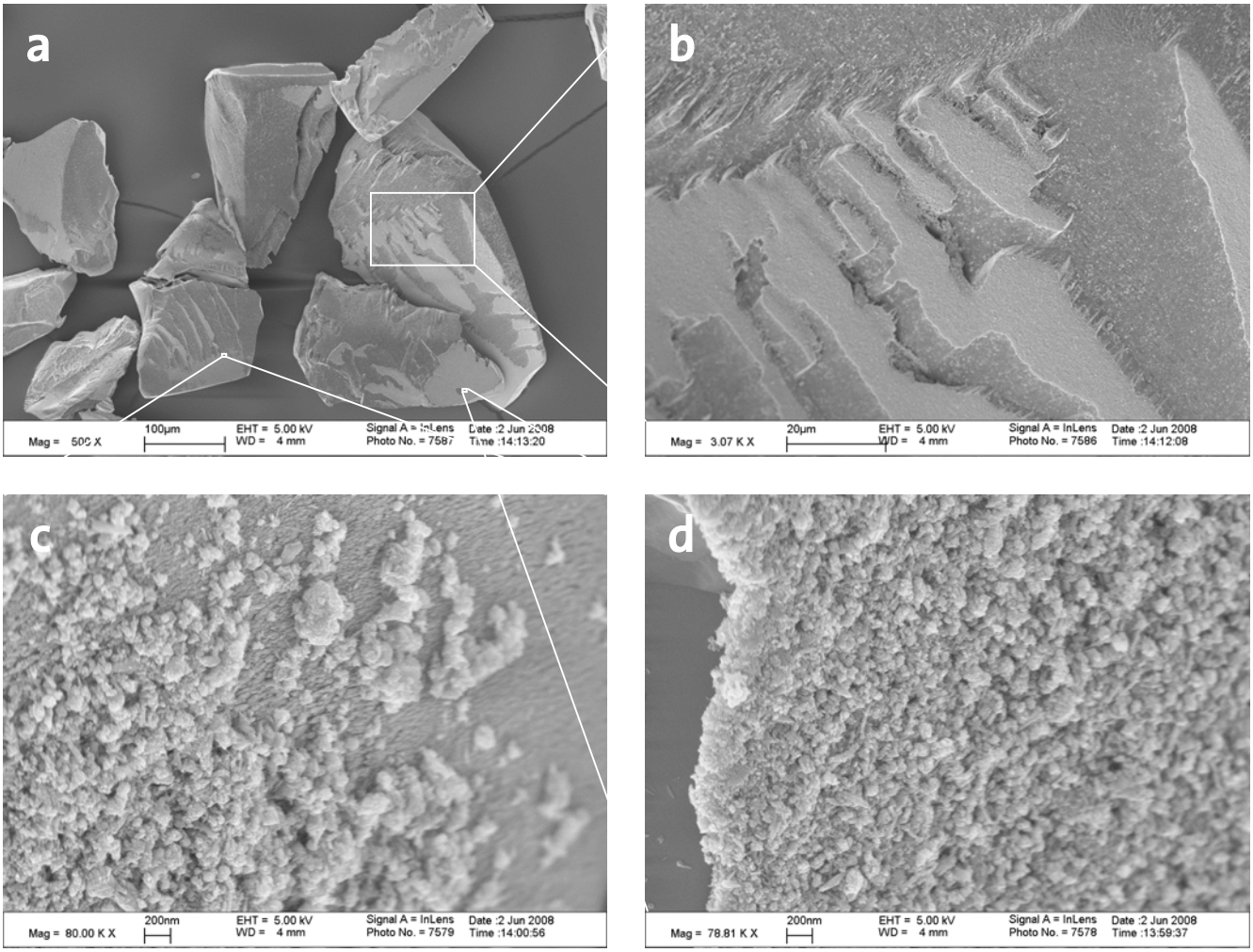

Figure 4-11: SEM images of reacted olivine from experiment R144, 11 h 1 min in CFSTR mode with m_o = 749 mg; for comparison with SEM images of unreacted olivine, see Fig. 4-2 on p. 25.

Sample dilution and ICP-OES analysis to measure the Mg concentration

Since EQ3/6 simulations showed that the amount of Mg complexes increases at high concentrations, five samples were selected from the sample collector, diluted by factor 20 and remeasured using the IC. Besides the Mg concentration profiles measured in-line and – upon dilution – off-line, Fig. 4-12 shows two additional data series. The first represents the in-line Mg concentrations corrected for the presence of complexes at measuring conditions that was calculated with EQ3/6. The second shows the results from the analysis by ICP-OES for a selection of five samples.

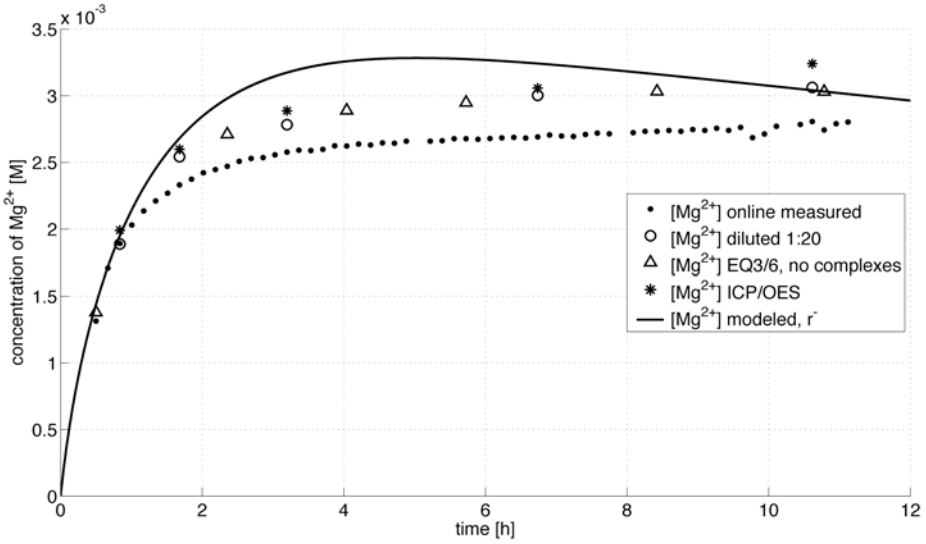

Figure 4-12: Concentration of Mg^{2+} over time from experiment R144, 11 h 1 min in CFSTR mode with m_o = 749 mg; comparison of different measuring methods, solid line represents modeled concentration (using r^-) of total magnesium, i.e. no complexes considered.

Confirmation of invalidity of in-line measuring

Fig. 4-12 proofs that for Mg concentrations higher than 2mM on-line measuring is indeed biased, owing to the presence of complexes. The two new measuring methods and the EQ3/6 based correction are in good agreement to each other. Appendix 7 contains also the comparison between the spectrophotometrical 5-sulfosalicyclic acid method used for Fe analysis and the corresponding results from ICP-OES.

Dissolution stoichiometry for experiment R144

Using the thus corrected Mg concentrations to plot the dissolution stoichiometry in the same way as done in Fig. 4.6 is shown in Fig. 4-13:

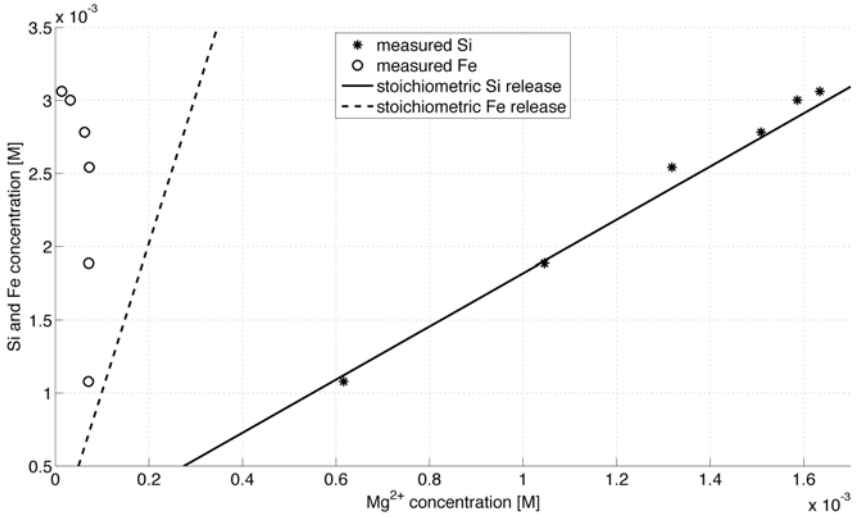

Figure 4-13: Measured concentrations of Fe and Si against Mg measurements (diluted samples) for experiment R144, 11 h 1 min in CFSTR mode with m_o = 749 mg; solid and dashed lines represent stoichiometric release for Si and Fe, respectively.

Proof of the absence of Mg bearing precipitates

Ionic iron was almost entirely removed from the system as the experiment proceeded, resulting in a strongly sub-stoichiometric Fe:Mg ratio. Silicon instead was not present in excess, as suggested by Fig. 4-6 for experiment R139. The Si release was either exactly congruent or slightly over-stoichiometric throughout the experiment. Hence, neither silica nor magnesium precipitates did form during this long run for 11 h. It follows that all secondary phases seen in the SEM images above consist of iron-oxides and/or hydroxides.

Possibly hindered dissolution by precipitation of Fe-oxides on olivine surface

Since the modeled concentrations start to be lower than the measurements, it seems that a threshold has been found where the general dissolution rate does not apply anymore. After excluding the precipitation of magnesite, the reason for this must be the partial coating of the olivine surface with Fe-rich precipitates. More experiments are needed to confirm this hypothesis.

Forced stop of experimental work

Unfortunately, the defective pump and subsequent set-up problems inhibited to continue with the experimental series. The only additional results shown here on the next page in Fig. 4-14 are SEM images of the last run, R145. A tenfold increase of the initial olivine mass (m_o = 7500 mg) resulted in the formation of many small single precipitates on the olivine surface, although the experiment was stirred at 700 rpm. The Mg concentration level reached not more than 4.5 mM, i.e. it was close to the profile measured during the carbonation experiment C2. However, the liquid level in the reactor decreased to 150 ml, thus the experiment would have to be repeated. This will be the starting point for future work.

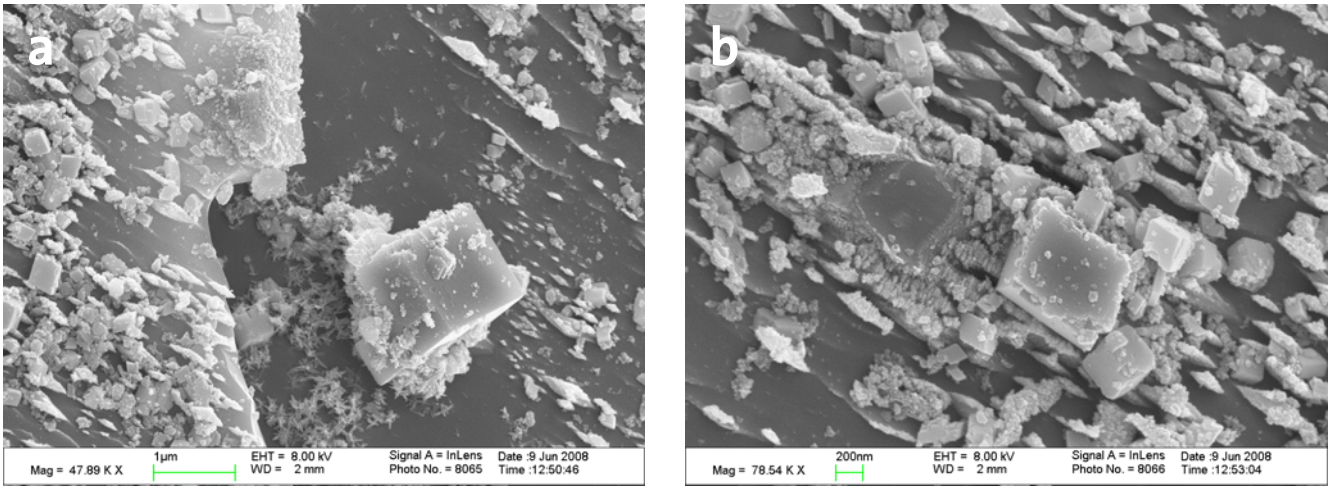

Figure 4-14: SEM images of reacted olivine from experiment R145, 9 h 25 min in CFSTR mode with m_o = 7502 mg; subplot (a) shows the co-precipitation of different solid phases on top of each other, subplot (b) shows that bigger particles can detach and leave fresh olivine surface for further dissolution (white arrow); for comparison with SEM images of unreacted olivine, see Fig. 4-2 on p. 25.

5. Conclusions

By developing a population balance equation model, the aqueous mineral carbonation process was simulated. Owing to the lack of empirical kinetic parameters, the model was used to gain a physical insight on a conceptual basis. By applying a wide range of temperature, CO_2 pressure and particle size, the model sensitivity regarding these parameters was tested. This revealed the model to be most sensitive to the reactor temperature and increasing the CO_2 pressure does not accelerate the onset of magnesite. Furthermore, the sensitivity analysis indicated that operating conditions of 120°C and 100 bar CO_2 pressure are possibly too mild to effectively sequester CO_2 in the H_2O-CO_2-olivine system.

The model failed to describe measured magnesium concentrations in carbonation experiments with an initial solid-liquid ratio of 5%. As a possible reason for this, the invalidity of the dissolution rate proposed by Hänchen et al. (2006/2207) could be excluded. The rate was confirmed in experiments where magnesium has been measured in similar concentrations as used for the regression in their study. By raising the solid-liquid ratios, it was found that the model starts to overestimate the measurements when the Mg concentration reaches a level of 3 mM. Simulations with the geochemical software package EQ3/6 revealed very high supersaturation ratios with respect to Fe oxides, whose precipitation was confirmed by a orange-brownish appearance of the reacted particles and by a coarse coating on parts of the olivine surface, as seen in SEM images. Dissolution was measured to be congruent for Mg and Si. Hence, the precipitation of silica and Mg bearing solids such as magnesite could be excluded. Very low Fe:Mg ratios towards the end of an experiment indicated that most of the ionic Fe was removed by precipitation on the olivine surface. This could possibly hinder the dissolution, which would account for the discrepancy between modeled and measured Mg concentrations. More work is needed to investigate the effect of the Fe-rich coating on olivine dissolution, and thus on the performance of the aqueous mineral carbonation process.

References

Bachu, S., Gunter, W. D., Perkins, E.H., 1994. Aquifer disposal of CO_2: hydrodynamic and mineral trapping, *Energy Convers. Manage.* **35**(4), 269–279.

Béarat, H., McKelvy, M. J., Chizmeshya, A. V. G., Gormley, D., Nunez, R., Carpenter, R. W., Squires, K., Wolf, G. H., 2006. Carbon Sequestration via Aqueous Olivine Mineral Carbonation: Role of Passivating Layer Formation. *Environ. Sci. Technol.* **40**, 4802-4808.

Berner, R.A., Lasaga, A.C., 1989. Modeling the geochemical carbon cycle. *Sci. Am.* **260**, 74–81.

Chen, Y., Brantley, S. L., 2000. Dissolution of forsteritic olivine at 65°C and 2<pH<5. *Chem. Geol.* **165**, 267-281.

Dunsmore, H.E., 1992. A geological perspective on global warming and the possibility of carbon dioxide removal as calcium carbonate mineral. *Energy Convers. Manage.* **33**(5– 8), 565–572.

Giammar, D. E., Bruant, J. R. G., Peters, C. A., 2005. Forsterite dissolution and magnesite precipitation at conditions relevant for deep saline aquifer storage and sequestration of carbon dioxide. *Chemical Geology* **217**, 257-276.

Gunter, W.D., Perkins, E.H., McCann, T.J., 1993. Aquifer disposal of CO_2-rich gases: reaction design for added capacity. *Energy Convers. Manage.* **34**, 941–948.

Hänchen, M., Prigiobbe, V., Storti, G., Seward, T.M., Mazzotti, M., 2006. Dissolution kinetics of fosteritic olivine at 90–150°C including effects of the presence of CO_2. *Geochim. Cosmochim. Acta*, **70**, 4403–4416.

Hänchen, M., Krevor, S., Mazzotti, M., Lackner, K.S., 2007. Validation of a population balance model for olivine dissolution. *Chem. Eng. Sci.*, **62**, 6412–6422.

Hänchen, M., Prigiobbe, V., Baciocchi, R., and Mazzotti, M., 2008. Precipitation in the Mg-carbonate system--effects of temperature and CO_2 pressure. *Chem. Eng. Sci.* **63**, 1012-1028.

IPCC, 2005. IPCC Special Report on Carbon Dioxide Capture and Storage. Prepared by Working Group III of the Intergovernmental Panel on Climate Change. *Cambridge University Press*, Cambridge, United Kingdom and NewYork, NY, USA, 442 pp.

IPCC, 2007. Climate Change 2007: The Physical Science Basis. Contribution of Working Group I to the Fourth Assessment Report of the Intergovernmental Panel on Climate Change. *Cambridge University Press*, Cambridge, United Kingdom and New York, NY, USA, 996 pp.

IPCC, 2007. Climate Change 2007: Impacts, Adaptation and Vulnerability. Contribution of Working Group II to the Fourth Assessment Report of the Intergovernmental Panel on Climate Change. *Cambridge University Press*, Cambridge, UK, 976 pp.

Lackner, K.S., Wendt, C.H., Butt, D.P., Joyce, E.L., Sharp, D.H., 1995. Carbon-dioxide disposal in carbonate minerals. *Energy* **20**, 1153–1170.

Lasaga, A.C., 1981. Dynamic treatment of geochemical cycles: global kinetics. In: Lasaga, A.C., Kirkpatrick, R.J. (Eds.), Kinetics of Geochemical Processes. *Reviews in Mineralogy* **8**, 69–110.

Lide, D.R., 2007. CRC Handbook of chemistry and physics. 88th ed., B&T, Oxford. (Online accessed: www.hbcpnetbase.com , last visited: 24.08.2008).

McKelvy, M.J., Chizmeshya, A.V.G., Squires, K., Carpenter, R.W., Béarat, H., 2006. A novel approach to mineral carbonation: Enhancing carbonation while avoiding mineral pretreatment process cost. Arizona State University, DE-FG26-04NT42124, annual report.

Mersmann, A., Ed., 2001. Crystallization Technology Handbook. 2nd ed., Marcel Dekker Inc., New York.

Nordstrom, D.K., Munoz, J.L., 1994. Geochemical thermodynamics. 2nd ed., Blackwell Scientific Publications, Cambridge, MA.

O'Connor, W.K., Dahlin, D.C., Rush, G.E., Gerdemann, S.J., Penner, L.R., Nilsen, D.N., 2004. Aqueous mineral carbonation: Mineral availability, pretreatment, reaction parametrics, and process studies. Albany Research Center, DOE/ARC-TR-04-002, interim report.

O'Connor, W. K., Dahlin, D. C., Rush, G. E., Gerdemann, S. J., Penner, L. R., Rubin, E. S., Keith, D. W., Gilboy, C. F., Wilson, M., Morris, T., Gale, J., and Thambimuthu, K., 2005. Energy and economic evaluation of ex situ aqueous mineral carbonation. *Greenhouse Gas Control Technologies 7*. Elsevier Science Ltd, Oxford.

Oelkers, E. H., 2001. An experimental study of forsterite dissolution rates as a function of temperature and aqueous Mg and Si concentrations. *Chemical Geology* **175**, 485-494.

Pokrovsky, O. S. and Schott, J., 2000. Kinetics and mechanism of forsterite dissolution at 25°C and pH from 1 to 12. *Geochim. Cosmochim. Acta* **64**, 3313-3325.

Randolph, A.; Larson, M. A., 1988.Theory of Particulate Processes. 2nd ed., Academic Press, San Diego, USA.

Rosso, J. J., Rimstidt, J. D., 2000. A high resolution study of forsterite dissolution rates. *Geochim. Cosmochim. Acta* **64**, 797-811.

Saltelli, A., Chan, K., Scott, E.M.,Eds., 2000. Sensitivity analysis. 1st ed., John Wiley & Sons Ltd, Chichester.

Schöll, J., Bonalumi, D., Vicum, L., Mazzotti, M., Müller, M., 2006. In Situ Monitoring and Modeling of the Solvent-Mediated Polymorphic Transformation of L-Glutamic Acid. *Cryst. Growth Des.* **6**, 881-891.

Seifritz, W., 1990. CO2 disposal by means of silicates. *Nature* **345**, 486.

Söhnel, O., Garside, J., 1992. Precipitation: Basic Principles and Industrial Applications. Butterworth-Heinemann, Oxford.

Wogelius, R. A., Walther, J. V., 1991. Olivine dissolution at 25°C: Effects of pH, CO2, and organic acids. *Geochimica et Cosmochimica Acta* **55**, 943-954.

Wolery, T.J., 1992. EQ3/6, a software package for geochemical modeling of aqueous systems: package overview and installation guide (version 8.0). Technical Report UCRL-MA-110662 PT I, Lawrence Livermore National Laboratory.

Appendices page

Appendix 1: Kinetic parameters for nucleation and growth

First set of visualized parameters for heterogeneous nucleation, corresponding to Eq. (35) on p. 8.

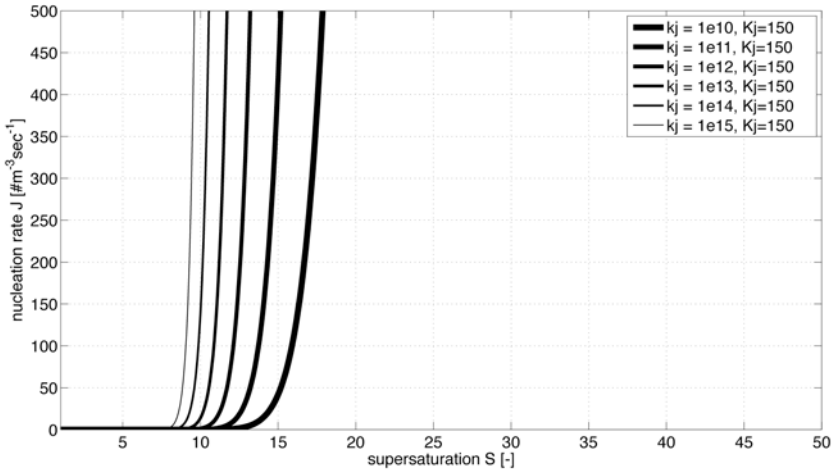

Second set of visualized parameters for heterogeneous nucleation, corresponding to Eq. (35) on p. 8. The dashed line corresponds to the parameters that were applied in the model.

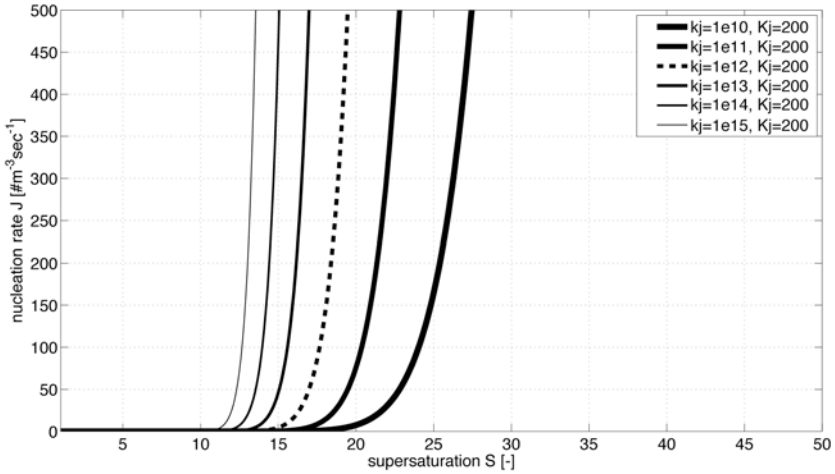

Third set of visualized parameters for heterogeneous nucleation, corresponding to Eq. (35) on p. 8.

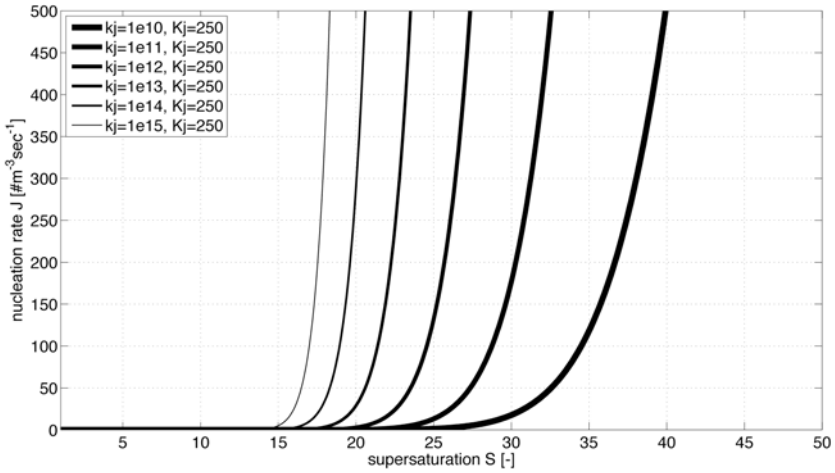

First set of visualized parameters for surface nucleation, corresponding to Eq. (37) on p. 8.

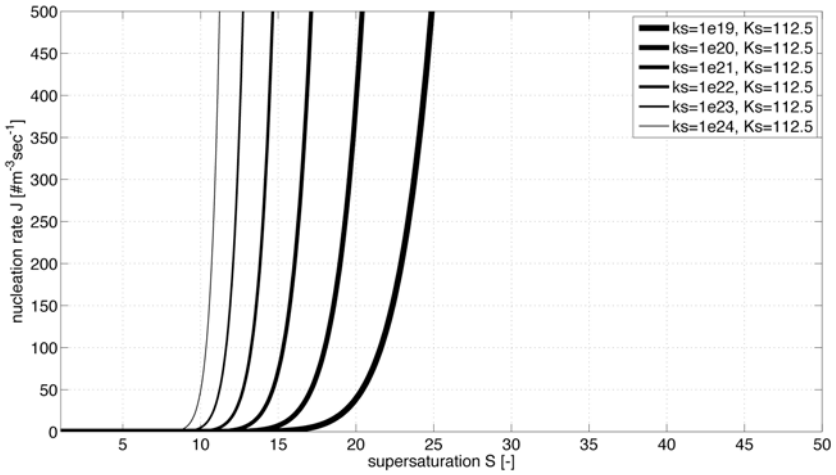

Second set of visualized parameters for surface nucleation, corresponding to Eq. (37) on p. 8. The dashed line corresponds to the parameters that were applied in the model.

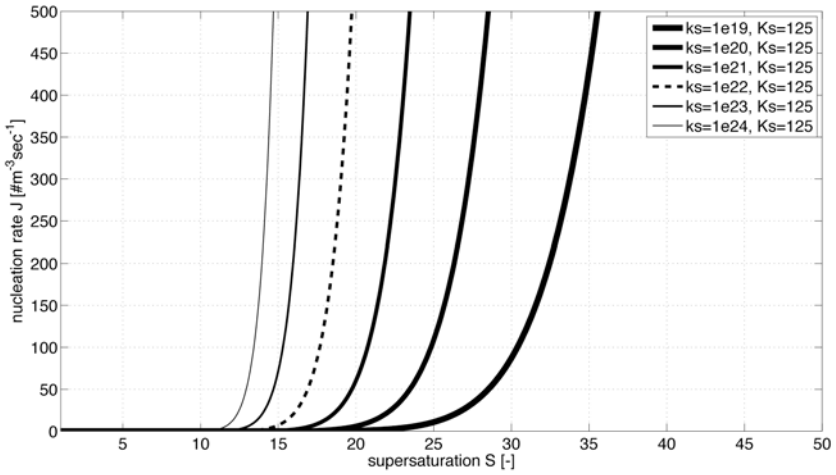

Third set of visualized parameters for surface nucleation, corresponding to Eq. (37) on p. 8.

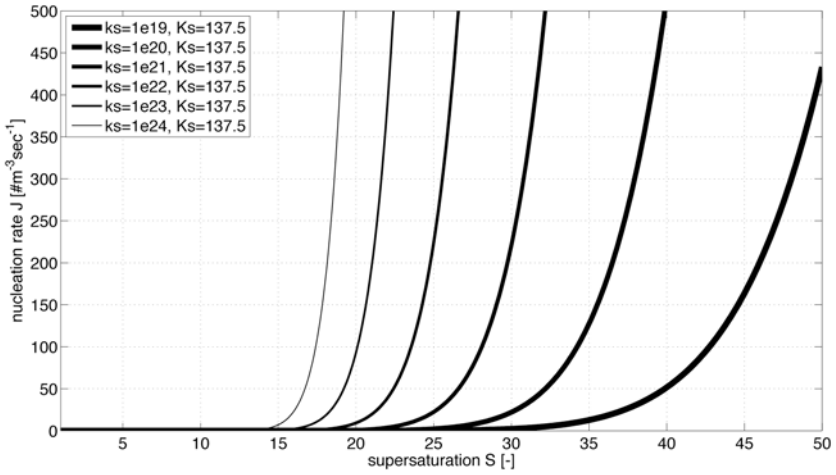

Appendix 2: Code

```
%% function runfile
% specifies the initial PSD (calling functions "loadCC" and normz_dist")and
% thermodynamic constants, calls the function "oliv_solvesetofodes" that
% initalizes the ODE solver, input parameters come from the function
% "visuals" that was introduced to hand over specific conditions for each
% experiment.
% written by Mischa Werner, in March 2008
% latest update: 25.08.2008

% notations: if material = wollastonite
%               a / (1) / woll = Wollastonite
%               b / (2) / calc = Calcite
%            if material = olivine
%               a / (1) / oliv = Olivine
%               b / (2) / magn = Magnesite

function runfile(material,Vri,Qi,Nai,Cli,massi,Ti,Pi,beti,meani,vari)

global Vr Q c_Na c_Cl T P_CO2
global c_ini rhom kv gamma_woA0 mass
global aBET dl l mean n0a n0anorm
global k
global K1 K2 K3 K4 K5 K6 K7 K8 K9 K10 K11 K12 K_25


%--------------- handing over the variables ------------------------------
Vr = Vri;                                              %solution volume [l]
Qml = Qi;                                  %flow rate for CSTR mode [ml/min]
Q = Qml/1000/60;                                                  %[l/sec]
c_Na = Nai;                                             %Sodium conc. [M]
c_Cl = Cli;                                            %Chlorid conc. [M]
mass = massi;                           %initital mass in to reactor [g]
% ratio = rati;                                    %solid liquid ratio [-]
T = Ti;                                          %reactor temperature [°K]
P_CO2 = Pi;                               %CO2 pressure in reactor [bar]
bet = beti;                              %BET-surface area of solute [m2/g]
mean = meani;                                 %mean particle diameter [m]


%%%%%%%%%%%%%%%%%%%%%%%%%%%%%%%%%%%%%%%%%%%%%%%%%%%%%%%%%%%%%%%%%%%%%%%%%%%
if strcmp(material,'woll')                                % wollastonite chosen

    disp('Nope, wollastonite comes later')

%%%%%%%%%%%%%%%%%%%%%%%%%%%%%%%%%%%%%%%%%%%%%%%%%%%%%%%%%%%%%%%%%%%%%%%%%%%
elseif strcmp(material,'oliv')                                % olivine chosen

%     %--------- reactor filling quantities if solid/liquid ratio based ---
%     rhos = [3320 1000];          %density of olivine and pure water [g/l]
%     Vmat = ratio*rhos(2)*Vr/(rhos(1)+ratio*rhos(2));  %olivine volume [l]
%     mass = Vmat*rhos(1);          %mass of olivine to fill in reactor [g]
%     Vwat = Vr-Vmat;                       %volume of water in reactor [l]
%     masswat = Vwat*rhos(2);                 %mass of water in reactor [g]

    %----------- sample/seed specification [olivine magnesite silica] -----
    m_inigram = [mass 0 0];    %initial mass of solute and precipitates [g]
    M = [146.408 108.6 60.1];                          %molar masses [g/mol]
    m_ini = m_inigram./M;       %init. mass of solute and precipitate [mol]
    c_ini = m_ini/Vr;  %init. concentrations of solute and precipitates [M]

    aBET = [bet 0.126 1];                 %specific BET surface area [m2/g]
                                                    %Oliv. --> see visuals.m
                                  %Magn. (100-200 microns), Kr, Jordan2007
                                                      %amorphous silica
    rho = [3300 3010 2200];                                %densities [kg/m3]
    rhom = rho./(M/1000);                        %molar densities [mol/m3]
    kv = [pi/6 pi/6 pi/6];                  %volumetric shape vactors [-]
    gamma_woA0 = aBET.*M.*c_ini./(3*rhom.*kv);                    %[m5/mol]
```

```
                    %gamma_woA0 is a parameter to transform the dissolution
                     %rate from mol/m2/sec (common in literature) in  m/sec


    %----------- initial PSD for olivine as measured in Coulter Counter ---
%    sourc_mt = '90-180a_fexd';           %specifiying the source material
%    CC = loadCC(sourc_mt);              %loading the Coulter Counter data
%    [CC_y,CC_x,CC_m,CC_F] = normz_dist(CC);     %loading CC-PSD properties
%
%    dl = CC_y*1e-6;                              %resolution (bin-size) [m]
%    l = CC_x*1e-6;                                 %all particle sizes [m]
%    VtotCC = CC_m*1e-18;                %total Volume of sample in CC [m3]
%    n0CC = CC_F*1e6;                  %number density of sample in CC [#/m]
%    n0a = c_ini(1)/(VtotCC*rhom(1))*n0CC;     %scaled up initial PSD [#/m]


    %--------- init. PSD for olivine standarized to Rosin-Rammler dist. ---
%     bin = 1e-8;                                      %uniform bin size [m]
%     l = (0:bin:500e-6)';                            %all particle sizes [m]
%     dl = ones(length(l),1)*bin;                        %bin size vector [m]
      %mean = 107e-6;                          %mean to adjust manually [m]
      %var = 0.1*mean;                       %variance to adjust manually [m]
%     n0 = wblpdf(l*1e6,mean*1e6,(mean*1e6)^0.5); %rosinrammler pdf [#/mum]
%     n0norm = normpdf(l*1e6,mean*1e6,(mean*1e6)^0.5);    %normal pdf [#/m]
%     fa = c_ini(1)/(rhom(1)*kv(1)*((l).^3)'*((dl).*n0));    %scaling [m-3]
%     fanorm = c_ini(1)/(rhom(1)*kv(1)*((l).^3)'*((dl).*n0norm));   %[m^-3]
%     n0a = fa*n0;                %scaled up initial RR-PSD f(0,L) [#/m/m3]
%     n0anorm = fanorm*n0norm;%scaled up initial normal PSD f(0,L) [#/m/m3]

%     %fb = m_ini(2)/(rho(2)*kv(2)*(l.^3)*(dl*n0)');    %scaling factor [-]
%     %n0b = fb*n0;            % PSDzero of magnesite seeds, if added [#/m]
%
%     %fc = m_ini(3)/(rho(3)*kv(3)*(l.^3)*(dl*n0)');    %scaling factor [-]
%     %n0c = fc*n0;              % PSDzero of silica seeds, if added [#/m]

    %----------- kinetic parameters ----------------------------------------
    kdo = 1;             %pre-exp. factor of oliv. dissolution rate [m/sec]
    kjm = 1e12;         %pre-exp. factor of Magn. nucleationrate [#/m3/sec]
    Kjm = 2e2;         %exponential factor of Magnestie nucleation rate [-]
    kgm = 2.5e-7;         %pre-exp. factor of Magnestie growth rate [m/sec]
    Kgm = 9e-2;            %exponential factor of Magnesite growth rate [-]
    ksm = 1e22;     %pre-exp. factor of Magn. surface nucleation [#/m3/sec]
    Ksm = 2e2;      %exponential factor of Mag. surface nucleation rate [-]
    kjs = 1e12;        %pre-exp. factor of silica nucleationrate [#/m3/sec]
    Kjs = 2e2;        %exponential factor of am. silica nucleation rate [-]
    kgs = 2.5e-7;      %pre-exp. factor of amor. silica growth rate [m/sec]
    Kgs = 9e-2;          %exponential factor of am. silica growth rate [-]
    kss = 1e22;    %pre-exp. factor of silica surface nucleation [#/m3/sec]
    Kss = 2e2;     %exponential factor of am. silica surface nucleation [-]

    k = [kdo kjm Kjm kgm Kgm ksm Ksm kjs Kjs kgs Kgs kss Kss];


    %----------- Calculating the equilibrium constants for olivine --------
    %----------- See file Thermodynamics.xls for origin of data -----------

    %    I: K1 = CO2(aq) / P_CO2 ---------------- solubility of CO2 in water
    %   II: K2 = HCO3(aq) * H(aq) / CO2(aq) --------- dissociation of H2CO3
    %  III: K3 = CO3(aq) * H(aq) / HCO3(aq) --------- dissociation of HCO3-
    %   IV: K4 = OH(aq) * H(aq) ---------------------- dissociation of water
    %    V: K5 = Mg(aq)*CO3(aq) -------------------- solubility of Magnesite
    %   VI: K6 = Mg(aq)^2*Si(OH)4(aq)*OH(aq)^4 --------- solubility of oliv
    %  VII: K7 = Si(OH)4(aq)/(SiO2(am)*H2O^2) ------- hydrolysis am. silica
    % VIII: K8 = SiO(OH)3(aq)*H(aq)/Si(OH)4(aq) ---- dissociation of H4SiO4
    %   IX: K9 = MgHCO3+(aq)/Mg(aq)*HCO3(aq) -------- solubility of MgHCO3+
    %    X: K10= MgCO3(aq)/(Mg(aq)*CO3(aq)) -------- formation of MgCO3(aq)
    %   XI: K11= (Fe3+(aq)^2*H2O^3)/(Fe2O3*H+^6) ------ solubility of Fe2O3
    %  XII: K12= Si(OH)4(aq)/(SiO2(s)*H2O^2) --------- hydrolysis of quartz

    %----------- standard eq. constants at 25∞C for olivine ---------------
    K1_25 = 10^(-1.4717);                                              %[-]
```

```
    K2_25 = 10^(-6.3598);                                                  %[-]
    K3_25 = 10^(-10.3369);                                                 %[-]
    K4_25 = 10^(-13.9987);                                                 %[-]
    K5_25 = 10^(-8.2170);                                                  %[-]
    K6_25 = 10^(-27.0863);                                                 %[-]
    K7_25 = 10^(-2.6981);                                                  %[-]
    K8_25 = 10^(-9.8113);                                                  %[-]
    K9_25 = 10^(1.0705);                                                   %[-]
    K10_25= 10^(2.9784);                                                   %[-]
    K11_25= 10^(0.10860);                                                  %[-]
    K12_25= 10^(-3.7668);                                                  %[-]

    K_25 = [K1_25 K2_25 K3_25 K4_25 K5_25 K6_25 K7_25 K8_25 K9_25 ...
        K10_25 K11_25 K12_25];                                             %[-]

    %----------- standard deltaH° at 25°C for olivine ---------------------
    delH0fK1 = -4.720;                                                 %[kcal/mol]
    delH0fK2 = 2.189;                                                  %[kcal/mol]
    delH0fK3 = 3.513;                                                  %[kcal/mol]
    delH0fK4 = 13.34;                                                  %[kcal/mol]
    delH0fK5 = -7.362;                                                 %[kcal/mol]
    delH0fK6 = 1.185;                                                  %[kcal/mol]
    delH0fK7 = 3.337;                                                  %[kcal/mol]
    delH0fK8 = 6.119;                                                  %[kcal/mol]
    delH0fK9 = 0.789;                                                  %[kcal/mol]
    delH0fK10= 2.713;                                                  %[kcal/mol]
    delH0fK11= -31.14;                                                 %[kcal/mol]
    delH0fK12= 5.99;                                                   %[kcal/mol]

    %----------- Van't Hoff equations -------------------------------------
    R = 1.987*10^-3;                %universal gas constant [kcal mol-1 K-1]
    K1 = K1_25*exp(-delH0fK1/R*(1/T-1/298.15));                            %[-]
    K2 = K2_25*exp(-delH0fK2/R*(1/T-1/298.15));                            %[-]
    K3 = K3_25*exp(-delH0fK3/R*(1/T-1/298.15));                            %[-]
    K4 = K4_25*exp(-delH0fK4/R*(1/T-1/298.15));                            %[-]
    K5 = K5_25*exp(-delH0fK5/R*(1/T-1/298.15));                            %[-]
    K6 = K6_25*exp(-delH0fK6/R*(1/T-1/298.15));                            %[-]
    K7 = K7_25*exp(-delH0fK7/R*(1/T-1/298.15));                            %[-]
    K8 = K8_25*exp(-delH0fK8/R*(1/T-1/298.15));                            %[-]
    K9 = K9_25*exp(-delH0fK9/R*(1/T-1/298.15));                            %[-]
    K10 = K10_25*exp(-delH0fK10/R*(1/T-1/298.15));                         %[-]
    K11 = K11_25*exp(-delH0fK11/R*(1/T-1/298.15));                         %[-]
    K12 = K12_25*exp(-delH0fK12/R*(1/T-1/298.15));                         %[-]

%     Kall = [K1 K2 K3 K4 K5 K6 K7 K8 K9 K10 K11 K12];
%     logKall = log10(Kall);

    %------------ running the function oliv_solvesetofodes ----------------
    answ = oliv_solvesetofodes;

end

%%%%%%%%%%%%%%%%%%%%%%%%%%%%%%%%%%%%%%%%%%%%%%%%%%%%%%%%%%%%%%%%%%%%%%%
%%%%%%%%%%%%%%%%%%%%%%%%%%%%%%%%%%%%%%%%%%%%%%%%%%%%%%%%%%%%%%%%%%%%%%%
%%%%%%%%%%%%%%%%%%%%%%%%%%%%%%%%%%%%%%%%%%%%%%%%%%%%%%%%%%%%%%%%%%%%%%%


%% function oliv_solvesetofodes
% specifies all initial conditions, calling the function "calcpH0open",
% and calls the ODE solver ode15s, a solver for stiff problems.
% secondly, it contains the code for result plotting, including the call of
% function "stoichiometry", for a better visualization of the dissolution
% written by Mischa Werner, in March 2008
% latest update: 25.08.2008

function [output] =  oliv_solvesetofodes

global Vr Q c_Na c_Cl T P_CO2 k
global c_ini rhom kv aBET gamma_woA0 mu2aini mass
```

```
global dl l mean n0a n0anorm
global K1 K2 K3 K4 K5 K6 K7 K8 K9 K10 K_25
global t_vector Dt_vector Dtsum
global A_oliv_vector
global c_MgHCO3_vector c_MgCO3aq_vector c_SiOOH3_vector
global c_H_vector pH_vector c_HCO3_vector c_CO3_vector
global So_vector Sm_vector Ss_vector
global D_vector Gm_vector Gs_vector Jo_vector Jm_vector Js_vector
global c_Mg_vector c_Mgtot_vector c_SiOH4_vector c_Sitot_vector
global data
global c_MgHCO3meas_vector c_MgCO3aqmeas_vector c_SiOOH3meas_vector
global c_Hmeas_vector pHmeas_vector c_HCO3meas_vector c_CO3meas_vector
global c_Mgmeas_vector c_SiOH4meas_vector
global c_MgCO3


%--------------- setting the initial values -------------------------------
mu3aini = (l.^3)'*(dl.*n0a);                                          %[m3]
mu2aini = (l.^2)'*(dl.*n0a);                                          %[m2]
mu1aini = l'*(dl.*n0a);                                               %[m]
mu0aini = sum(dl.*n0a);                                               %[-]

mu3bini = 0;                                                          %[m3]
mu2bini = 0;                                                          %[m2]
mu1bini = 0;                                                          %[m]
mu0bini = 0;                                                          %[-]

mu3cini = 0;                                                          %[m3]
mu2cini = 0;                                                          %[m2]
mu1cini = 0;                                                          %[m]
mu0cini = 0;                                                          %[-]

c_Mg_totini = 0;                                                      %[M]
c_Si_totini = 0;                                                      %[M]

x0 = [mu3aini; mu2aini; mu1aini; mu0aini; mu3bini; mu2bini; mu1bini; ...
    mu0bini; mu3cini; mu2cini; mu1cini; mu0cini; c_Mg_totini; c_Si_totini];

[H0,pH0,OH0,HCO30,CO30]=calcpH0open(c_Na,c_Cl,P_CO2);
         %calculates the initial pH of solution for the system NaCl-CO2-H2O

t_vector = 0;                                                       %[sec]
Dt_vector = 0;                                                        %[m]
Dtsum = 0;                                                            %[M]
A_oliv_vector = mu2aini;                                             %[m2]
c_Mgtot_vector = 0;                                                   %[M]
c_Mg_vector = 0;                                                      %[M]
c_MgHCO3_vector = 0;                                                  %[M]
c_MgCO3aq_vector = 0;                                                 %[M]
c_Sitot_vector = 0;                                                   %[M]
c_SiOH4_vector = 0;                                                   %[M]
c_SiOOH3_vector = 0;                                                  %[M]
c_H_vector = H0;                                                      %[M]
pH_vector = pH0;                                                      %[-]
c_HCO3_vector = HCO30;                                                %[M]
c_CO3_vector = CO30;                                                  %[M]
So_vector = 0;                                                        %[-]
Sm_vector = 0;                                                        %[-]
Ss_vector = 0;                                                        %[-]
D_vector = 0;                                                     %[m/sec]
Gm_vector = 0;                                                    %[m/sec]
Gs_vector = 0;                                                    %[m/sec]
Jo_vector = 0;                                                  %[#/m3/sec]
Jm_vector = 0;                                                  %[#/m3/sec]
Js_vector = 0;                                                  %[#/m3/sec]

P_CO2meas = 3.85e-4;                                                %[bar]
[H0meas,pH0meas,OH0meas,HCO30meas,CO30meas] = calcpH0meas(c_Na,c_Cl, ...
    P_CO2meas);
c_Mgmeas_vector = 0;                                                  %[M]
c_MgHCO3meas_vector = 0;                                              %[M]
```

```
c_MgCO3aqmeas_vector = 0;                                          %[M]
c_SiOH4meas_vector = 0;                                            %[M]
c_SiOOH3meas_vector = 0;                                           %[M]
c_Hmeas_vector = H0meas*1000;                                     %[mM]
pHmeas_vector = pH0meas;                                           %[-]
c_HCO3meas_vector = HCO30meas*1000;                               %[mM]
c_CO3meas_vector = CO30meas*1000;                                 %[mM]


%--------------- running the ODEs solver for olivine ----------------------
tspan = [0 3*3600];                                              %[sec]

options = odeset('MaxStep',5,'InitialStep',1,'RelTol',1e-3, ...
                 'OutputFcn','vectors');
%options = [];

[t,x] = ode15s(@oliv_setofodes,tspan,x0,options);

output = [t x];
X = real(x);                                 %filtering imaginary parts
X = (X+abs(X))/2;                            %filtering negative values
time = t/3600;                                                     %[h]


%--------------- calculating the final amounts ----------------------------
c_Mg2SiO4 = rhom(1)*kv(1)*X(:,1);            %mass of remaining olivine [M]
c_MgCO3 = rhom(2)*kv(2)*X(:,5);          %mass of precipitated magnesite [M]
c_SiO2 = rhom(3)*kv(3)*X(:,9);         %conc. of precipitated am. silica [M]
c_Mgtot = X(:,13);                          %total magnesium in solution [M]
c_Sitot = X(:,14);                            %total silicon in solution [M]
end

%%%%%%%%%%%%%%%%%%%%%%%%%%%%%%%%%%%%%%%%%%%%%%%%%%%%%%%%%%%%%%%%%%%%%%%%%%%%

%%%%%%%%%%%%%%%%%%%%%%%%%%%%%%%%%%%%%%%%%%%%%%%%%%%%%%%%%%%%%%%%%%%%%%%%%%%%

%%%%%%%%%%%%%%%%%%%%%%%%%%%%%%%%%%%%%%%%%%%%%%%%%%%%%%%%%%%%%%%%%%%%%%%%%%%%


%% function oliv_setofodes
% contains the set of ODEs that follow from solving the Population Balance
% Equations using the method of moments; additionally, 2 ODEs account for
% mass balance for magnesium and silicon in solution
% written by Mischa Werner, in March 2008
% latest update: 25.08.2008

function [dxdt] = oliv_setofodes(t,x)

global Vr Q c_Na c_Cl T P_CO2 k
global c_ini rhom kv aBET gamma_woA0 mu2aini mass
global dl l mean n0a
global K1 K2 K3 K4 K5 K6 K7 K8 K9 K10
global t_vector Dt_vector Dtsum
global A_oliv_vector
global c_MgHCO3_vector c_MgCO3aq_vector c_SiOOH3_vector
global c_H_vector pH_vector c_HCO3_vector c_CO3_vector
global So_vector Sm_vector Ss_vector
global D_vector Gm_vector Gs_vector Jo_vector Jm_vector Js_vector
global c_Mg_vector c_Mgtot_vector c_SiOH4_vector c_Sitot_vector
global data


%--------------- handing over the results from previous step --------------
mu3a = x(1); mu2a = x(2); mu1a = x(3); mu0a = x(4); ...
    mu3b = x(5); mu2b = x(6); mu1b = x(7); mu0b = x(8); ...
        mu3c = x(9); mu2c = x(10); mu1c = x(11); mu0c = x(12); ...
            c_Mgtot = x(13); c_Sitot = x(14);

%--------------- finding the length in the initial PSD corresponding to ---
%--------------- the currently dissolved amount of olivine ----------------
p = (l - ones(length(l),1)*Dtsum);
a = find(abs(p) == min(abs(p)));
```

```
%--------------- set of the 12 moments ----------------------------------
dmu0adt = -D_vector(end)*n0a(a)+ Jo_vector(end);
dmu1adt = -D_vector(end)*mu0a;
dmu2adt = -2*D_vector(end)*mu1a;
dmu3adt = -3*D_vector(end)*mu2a;

dmu3bdt = 3*Gm_vector(end)*mu2b;
dmu2bdt = 2*Gm_vector(end)*mu1b;
dmu1bdt = Gm_vector(end)*mu0b;
dmu0bdt = Jm_vector(end);

dmu3cdt = 3*Gs_vector(end)*mu2c;
dmu2cdt = 2*Gs_vector(end)*mu1c;
dmu1cdt = Gs_vector(end)*mu0c;
dmu0cdt = Js_vector(end);

%--------------- material balances ---------------------------------------
dc_Mgtotdt =-1.82*rhom(1)*kv(1)*dmu3adt-rhom(2)*kv(2)*dmu3bdt-Q/Vr*c_Mgtot;
dc_Sitotdt = -rhom(1)*kv(1)*dmu3adt - rhom(3)*kv(3)*dmu3cdt - Q/Vr*c_Sitot;

%--------------- passing over the solution from current step --------------
dxdt = [dmu3adt; dmu2adt; dmu1adt; dmu0adt; dmu3bdt; dmu2bdt; dmu1bdt; ...
      dmu0bdt; dmu3cdt; dmu2cdt; dmu1cdt; dmu0cdt; dc_Mgtotdt; dc_Sitotdt];


%%%%%%%%%%%%%%%%%%%%%%%%%%%%%%%%%%%%%%%%%%%%%%%%%%%%%%%%%%%%%%%%%%%%%%%
%%%%%%%%%%%%%%%%%%%%%%%%%%%%%%%%%%%%%%%%%%%%%%%%%%%%%%%%%%%%%%%%%%%%%%%
%%%%%%%%%%%%%%%%%%%%%%%%%%%%%%%%%%%%%%%%%%%%%%%%%%%%%%%%%%%%%%%%%%%%%%%


%% built-in function vectors
% is the built-in output function for the ode15s solver called within the
% function olive_solvesetofodesof. calls function oliv_rates and returns
% all parameters such as rates and complex-concentrations whenever the
% solver adds an integration step to the solution matrix x.
% written by Mischa Werner in June, 2008
% latest update: 25.08.2008

function status = vectors(t,x,flag)

global Vr Q c_Na c_Cl T P_CO2 k
global c_ini rhom kv aBET gamma_woA0 mu2aini mass
global dl l mean n0a
global K1 K2 K3 K4 K5 K6 K7 K8 K9 K10 K_25
global t_vector Dt_vector Dtsum
global A_oliv_vector
global c_MgHCO3_vector c_MgCO3aq_vector c_SiOOH3_vector
global c_H_vector pH_vector c_HCO3_vector c_CO3_vector
global So_vector Sm_vector Ss_vector
global D_vector Gm_vector Gs_vector Jo_vector Jm_vector Js_vector
global c_Mg_vector c_Mgtot_vector c_SiOH4_vector c_Sitot_vector
global data
global c_MgHCO3meas_vector c_MgCO3aqmeas_vector c_SiOOH3meas_vector
global c_Hmeas_vector pHmeas_vector c_HCO3meas_vector c_CO3meas_vector
global c_Mgmeas_vector c_SiOH4meas_vector

flag = [];

%--------------- terminating the OutputFun call at end of integration -----
if numel(x) >= 1
    c_Mgtot = x(13);                                                  %[M]
    c_Sitot = x(14);                                                  %[M]
    A_oliv = x(2);                                                   %[m2]
else
    c_Mgtot = c_Mgtot_vector(end);                                    %[M]
    c_Sitot = c_Sitot_vector(end);                                    %[M]
    A_oliv = A_oliv_vector(end);                                     %[m2]
end
```

```
if length(t)>1
    t = t(1);                                                          %[sec]
end


if ((numel(t) ~= 0) && (t > 0))
    %----------- calculating free Mg2+, SiOH4 and complexes based on ------
    %----------- previous values for specification ----------------------
    c_H = c_H_vector(end);                                             %[M]
    c_HCO3 = c_HCO3_vector(end);                                       %[M]
    c_CO3 = c_CO3_vector(end);                                         %[M]

    c_Mg = c_Mgtot/(1 + c_HCO3*K9 + c_CO3*K10);                        %[M]
    c_SiOH4 = c_Sitot/(1 + K8/c_H);                                    %[M]

    c_MgHCO3 = c_Mg*c_HCO3*K9;                                         %[M]
    c_MgCO3aq = c_Mg*c_CO3*K10;                                        %[M]
    c_SiOOH3 = c_SiOH4*K8/c_H;                                         %[M]

    %----------- calculating current rates, pH, supersaturation -----------
    [S,R,J,H,pH,OH,HCO3,CO3] = oliv_rates(c_Mg,c_SiOH4,c_SiOOH3, ...
                               c_MgHCO3,P_CO2,k,gamma_woA0,mu2aini,A_oliv);

    %----------- determining the amount of olivine that has been ----------
    %----------- currently dissolved since the previous step --------------
    delta_t = t(end)-t_vector(end);
    Dt_step = abs(R(1)*delta_t);

    %----------- recording all current values that correspond to ----------
    %----------- a chosen current solution point -------------------------
    t_vector = [t_vector; t(end)];                                    %[sec]
    Dt_vector = [Dt_vector; Dt_step];                                   %[m]
    A_oliv_vector = [A_oliv_vector; A_oliv];                          %[m2]
    c_Mgtot_vector = [c_Mgtot_vector; c_Mgtot];                         %[M]
    c_Mg_vector = [c_Mg_vector; c_Mg];                                  %[M]
    c_MgHCO3_vector = [c_MgHCO3_vector; c_MgHCO3];                      %[M]
    c_MgCO3aq_vector = [c_MgCO3aq_vector; c_MgCO3aq];                   %[M]
    c_Sitot_vector = [c_Sitot_vector; c_Sitot];                         %[M]
    c_SiOH4_vector = [c_SiOH4_vector; c_SiOH4];                         %[M]
    c_SiOOH3_vector = [c_SiOOH3_vector; c_SiOOH3];                      %[M]
    c_H_vector = [c_H_vector; H];                                       %[M]
    pH_vector = [pH_vector; pH];                                        %[-]
    c_HCO3_vector = [c_HCO3_vector; HCO3];                              %[M]
    c_CO3_vector = [c_CO3_vector; CO3];                                 %[M]
    So_vector = [So_vector; S(1)];                                      %[-]
    Sm_vector = [Sm_vector; S(2)];                                      %[-]
    Ss_vector = [Ss_vector; S(3)];                                      %[-]
    D_vector = [D_vector; R(1)];                                    %[m/sec]
    Gm_vector = [Gm_vector; R(2)];                                  %[m/sec]
    Gs_vector = [Gs_vector; R(3)];                                  %[m/sec]
    Jo_vector = [Jo_vector; J(1)];                                %[#/m3/sec]
    Jm_vector = [Jm_vector; J(2)];                                %[#/m3/sec]
    Js_vector = [Js_vector; J(3)];                                %[#/m3/sec]

    %----------- calculating current pH and conc. at measuring conditions -
    P_CO2meas = 3.85e-4;
    c_Hmeas = c_Hmeas_vector(end);                                     %[mM]
    c_HCO3meas = c_HCO3meas_vector(end);                               %[mM]
    c_CO3meas = c_CO3meas_vector(end);                                 %[mM]

    c_Mgtotmilli = 1000*c_Mgtot;                                       %[mM]
    c_Sitotmilli = 1000*c_Sitot;                                       %[mM]

    c_Mgmeas = c_Mgtotmilli/(1 + c_HCO3meas*K_25(9) + c_CO3meas*K_25(10));
    c_SiOH4meas = c_Sitotmilli/(1 + K_25(8)/(c_Hmeas));                %[mM]

    c_MgHCO3meas = c_Mgmeas*c_HCO3meas*K_25(9);                        %[mM]
    c_MgCO3aqmeas = c_Mgmeas*c_CO3meas*K_25(10);                       %[mM]
    c_SiOOH3meas = c_SiOH4meas*K_25(8)/c_Hmeas;                        %[mM]
```

```
    [Hmeas,pHmeas,HCO3meas,CO3meas] = oliv_calcpHmeas(c_Na,c_Cl, ...
        c_Mgmeas,c_SiOOH3meas,c_MgHCO3meas,P_CO2meas,c_Hmeas);

    c_Mgmeas_vector = [c_Mgmeas_vector; c_Mgmeas];                    %[mM]
    c_MgHCO3meas_vector = [c_MgHCO3meas_vector; c_MgHCO3meas];        %[mM]
    c_MgCO3aqmeas_vector = [c_MgCO3aqmeas_vector; c_MgCO3aqmeas];     %[mM]
    c_SiOH4meas_vector = [c_SiOH4meas_vector; c_SiOH4meas];           %[mM]
    c_SiOOH3meas_vector = [c_SiOOH3meas_vector; c_SiOOH3meas];        %[mM]
    c_Hmeas_vector = [c_Hmeas_vector; Hmeas];                         %[mM]
    pHmeas_vector = [pHmeas_vector; pHmeas];                           %[-]
    c_HCO3meas_vector = [c_HCO3meas_vector; HCO3meas];                %[mM]
    c_CO3meas_vector = [c_CO3meas_vector; CO3meas];                   %[mM]

end

%--------------- determining the amount of olivine that has been ----------
%--------------- dissolved in total until the current step ----------------
Dtsum = sum(Dt_vector);

%--------------- status 0 = continue, status 1 =  stop after first --------
%--------------- timestep -------------------------------------------------
status = 0;


%%%%%%%%%%%%%%%%%%%%%%%%%%%%%%%%%%%%%%%%%%%%%%%%%%%%%%%%%%%%%%%%%%%%%%%%
%%%%%%%%%%%%%%%%%%%%%%%%%%%%%%%%%%%%%%%%%%%%%%%%%%%%%%%%%%%%%%%%%%%%%%%%
%%%%%%%%%%%%%%%%%%%%%%%%%%%%%%%%%%%%%%%%%%%%%%%%%%%%%%%%%%%%%%%%%%%%%%%%


%% function oliv_rates
% calls function oliv_calcpHopen and returns the values for Supersaturation
% and the rates for dissolution/nucleation/growth, and passes the
% values for H, pH, OH, HCO3, CO3 to the Output function "vectors"
% written by Mischa Werner in June, 2008
% latest update: 25.08.2008


function [S,R,J,H,pH,OH,HCO3,CO3] = oliv_rates(c_Mg,c_SiOH4,c_SiOOH3, ...
                                    c_MgHCO3,P_CO2,k,gamma_woA0,mu2aini,A_oliv)

global T c_Na c_Cl
global K1 K2 K3 K4 K5 K6 K7 K8 K9 K10


%--------------- calculating the H+ and pH --------------------------------
[H,pH] = oliv_calcpHopen(c_Na,c_Cl,c_Mg,c_SiOOH3,c_MgHCO3,P_CO2);

%--------------- calc. the current conc. already needed for Supersat. -----
OH = K4/H;                                                            %[M]
HCO3=K2*K1*P_CO2/H;                                                   %[M]
CO3 = K3*HCO3/H;                                                      %[M]

%--------------- calc. the Supersaturations -------------------------------
So = ((c_Mg^2*c_SiOH4*OH^4)/K6)^(1/7);                                 %[-]
Sm = ((c_Mg*CO3)/K5)^(1/2);                                           %[-]
Ss = c_SiOH4/K7;                                                      %[-]
S = [So Sm Ss];                                                       %[-]

%--------------- dissolution olivine --------------------------------------
 if So < 1
    R = 8.314472;                       %universal gas constant [J mol-1 K-1]
    r = k(1)*10^(-0.46*pH-(52.9e3/(log(10)*R*T))-1.021+4);  %[molol/m2/sec]
                        %source: combination of Haenchen2006 and Haenchen2007
                %extrapolated from 120∞C to 90-150∞C, regressed at pH = 2-6.5

%     r = k(1)*10^(-0.43*pH-(52.9e3/(log(10)*R*T))-0.89+4); %[molol/m2/sec]
%                                           error band: fastest dissolution
%     r = k(1)*10^(-0.49*pH-(52.9e3/(log(10)*R*T))-1.15+4); %[molol/m2/sec]
%                                           error band: slowest dissolution
```

```
    D = r*gamma_woA0(1)/mu2aini;   %dissolution rate as used in PBE [m/sec]
else
    D = 0;
 end

%--------------- nucleation olivine ----------------------------------------
if So > 1
    Jo = 0;                                                          %[#/m3/s]
else
    Jo = 0;                                                          %[#/m3/s]
end

%--------------- heterogeneous nucleation magnesite -----------------------
if Sm > 1
    Jhm = k(2)*S(2)^(3/7)*exp(-k(3)/log(S(2))^2);                    %[#/m3/s]
else
    Jhm = 0;                                                         %[#/m3/s]
end

% %--------------- heterogeneous nucleation amorphous silica --------------
% if Ss > 1
%     Jhs = k(8)*S(3)^(3/7)*exp(-k(9)/log(S(3))^2);                  %[#/m3/s]
% else
%     Jhs = 0;                                                       %[#/m3/s]
% end

% %--------------- surface nucleation magnesite ---------------------------
% if Sm > 1
%     Jsm = k(6)*A_oliv*exp(-k(7)/(S(2)-1));                       % [#/m3/s]
% else
%     Jsm = 0;                                                     % [#/m3/s]
% end

%--------------- surface nucleation amorphous silica ----------------------
if Ss > 1
    Jss = k(12)*A_oliv*exp(-k(13)/(S(3)-1));                       % [#/m3/s]
else
    Jss = 0;                                                       % [#/m3/s]
end

%--------------- isotropic growth magnesite -------------------------------
if Sm > 1
    Gm = k(4)*(S(2)-1)^(5/6)*exp(-k(5)/(S(2)-1));                    %[m/sec]
else
    Gm = 0;                                                          %[m/sec]
end

%--------------- isotropic growth silica ----------------------------------
if Ss > 1
    Gs = k(10)*(S(3)-1)^(5/6)*exp(-k(11)/(S(3)-1));                  %[m/sec]
else
    Gs = 0;                                                          %[m/sec]
end

R = [D Gm Gs];                                                       %[m/sec]
J = [Jo Jhm Jss];                                                   %[#/m3/s]
% R = [D 0 0];                                                       %[m/sec]
% J=[0 0 0];                                                        %[#/m3/s]

%%%%%%%%%%%%%%%%%%%%%%%%%%%%%%%%%%%%%%%%%%%%%%%%%%%%%%%%%%%%%%%%%%%%%%%%%%%
%%%%%%%%%%%%%%%%%%%%%%%%%%%%%%%%%%%%%%%%%%%%%%%%%%%%%%%%%%%%%%%%%%%%%%%%%%%
%%%%%%%%%%%%%%%%%%%%%%%%%%%%%%%%%%%%%%%%%%%%%%%%%%%%%%%%%%%%%%%%%%%%%%%%%%%

%% function oliv_calcpHopen
% returns the solution to the charge balance for H
% written by Mischa Werner in June, 2008
% latest update: 25.08.2008
```

```
function [H,pH] = oliv_calcpHopen(c_Na,c_Cl,c_Mg,c_SiOOH3,c_MgHCO3,P_CO2)

global K1 K2 K3 K4 K5 K6 K7 K8 K9 K10

%-----------Coefficients of the Polynom-----------------------------------
C1=1;
C2=c_MgHCO3+2*c_Mg+c_Na-c_SiOOH3-c_Cl;
C3=-K4-K2*K1*P_CO2;
C4=-2*K3*K2*K1*P_CO2;

p=[C1 C2 C3 C4];
r=roots(p);

if r(1)>0
    H = r(1);      % [mol]
elseif r(2)>0
    H = r(2);      % [mol]
elseif r(3)>0
    H = r(3);      % [mol]
end

pH = -log10(H); % [-]
```

Appendix 3: Rosin-Rammler and Gaussian distribution

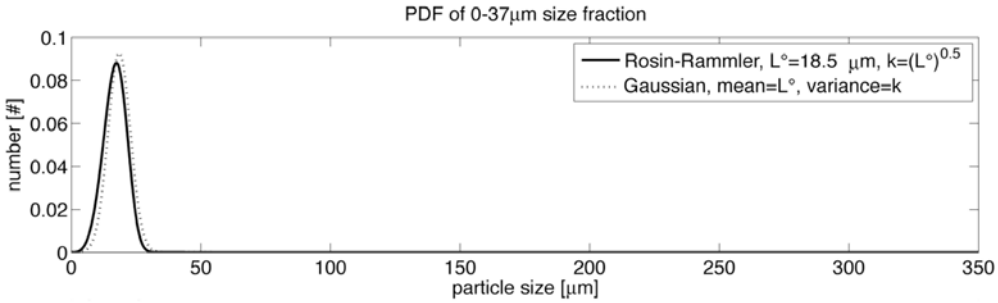

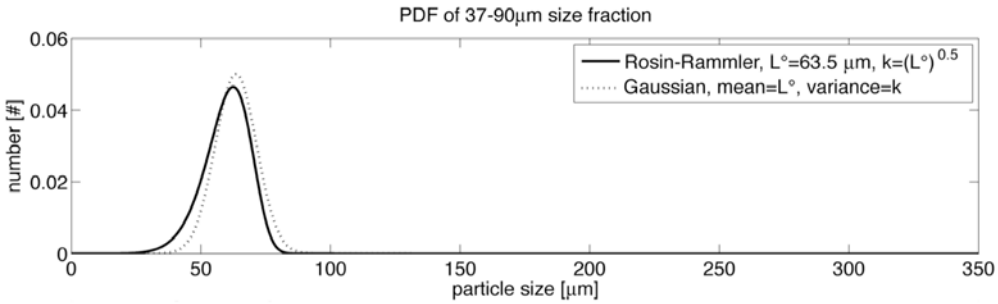

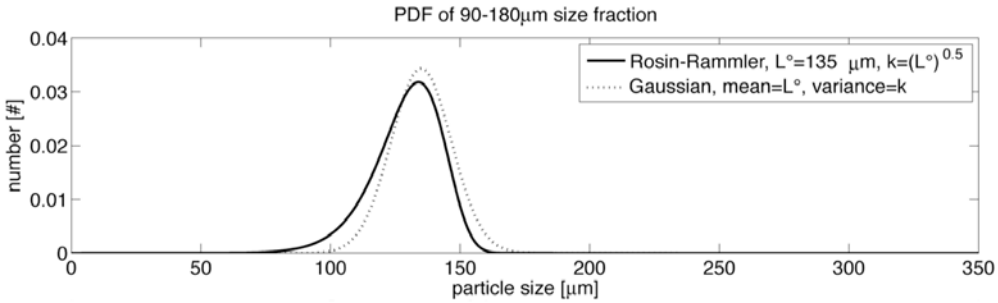

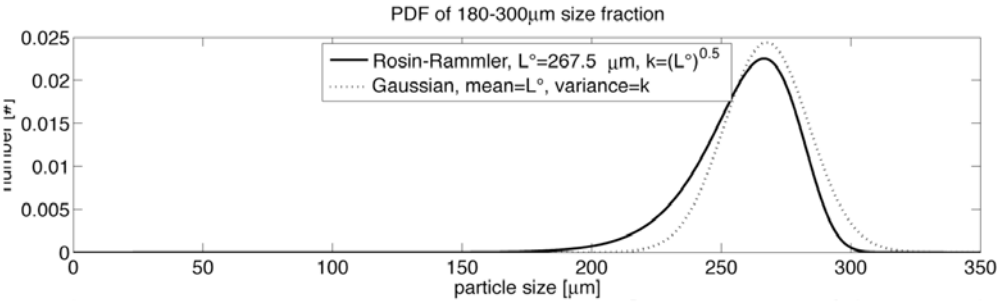

Appendix 4: Regression for BET surface area

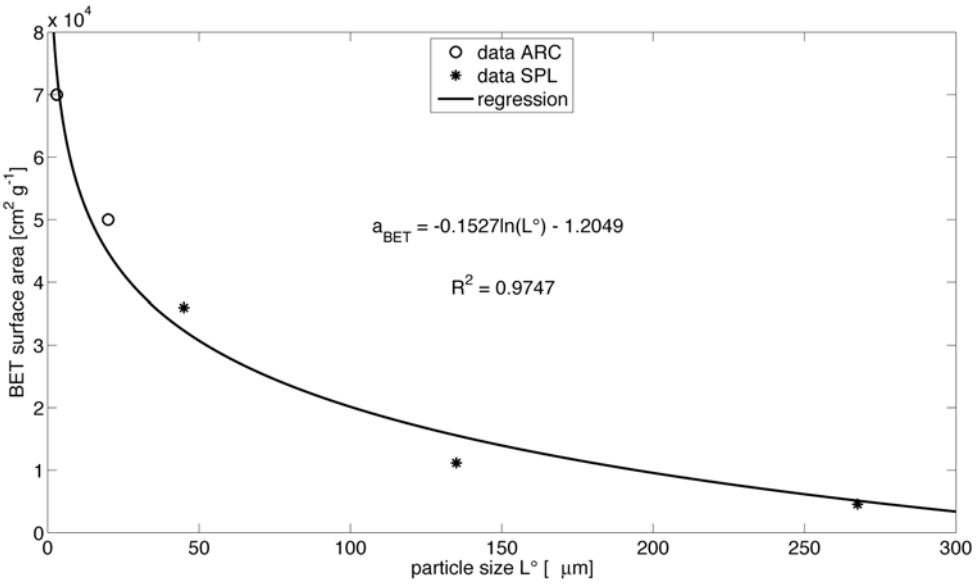

Appendix 5: Stirring

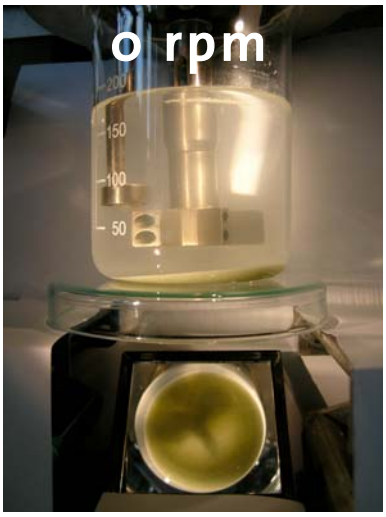

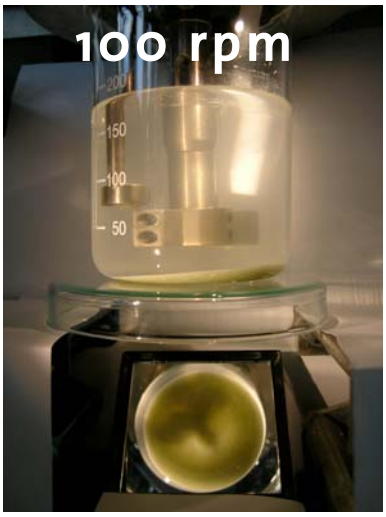

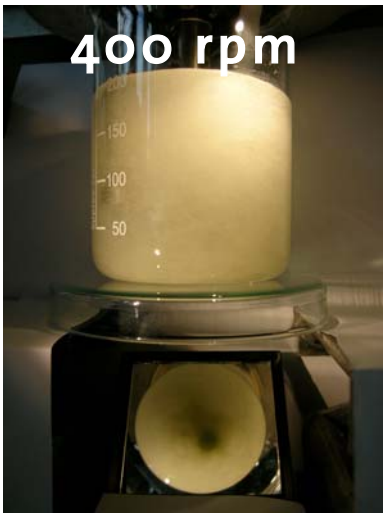

Effect of strirring rate on heat transfer:

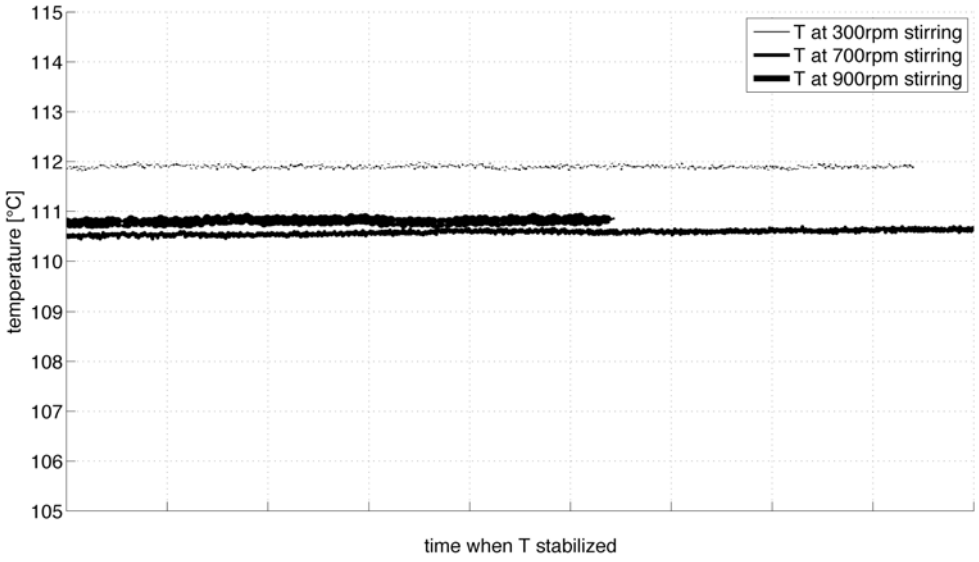

Appendix 6: Effect of Teflon cover on temperature measurement

With Teflon cover on:
Reactor temperature set to 120°C to record the mean T the oil bath has to have, while the cover is on.

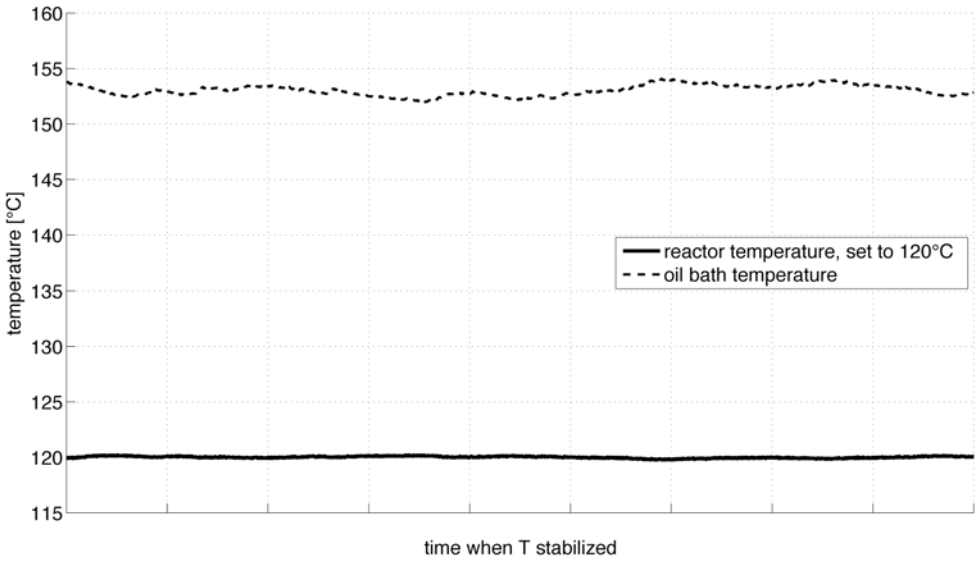

Without Teflon cover:
Oil bath temperature set to 152.5°C, the mean T to keep the reactor at 120°C when the cover is on (see plot above). The measured difference to 120°C is approx. 2°C.

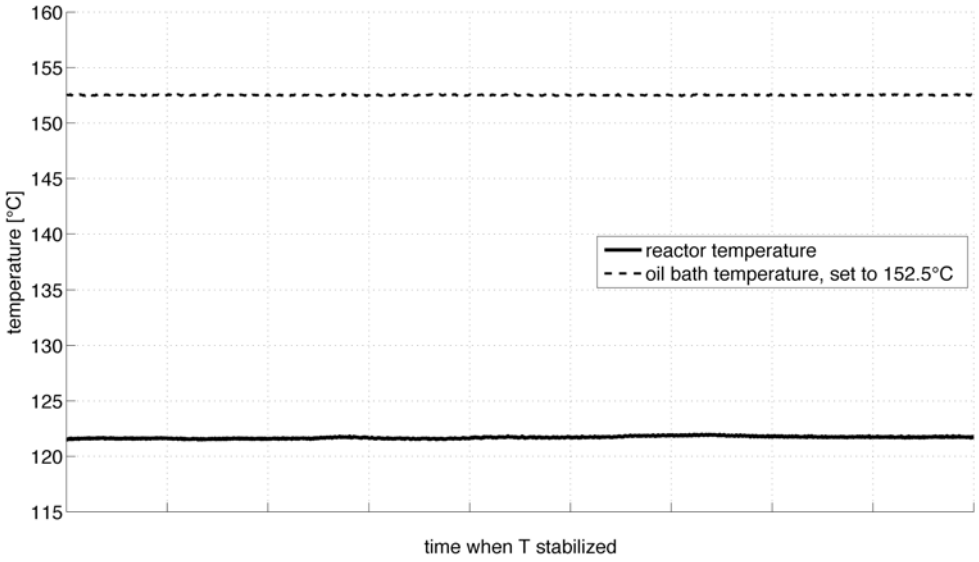

Appendix 7: Comparison ICP-OES with 5-sulfosalicyclic acid method